Journal of Energy Chemistry 90 (2024) 540–564

Contents lists available at ScienceDirect

Journal of Energy Chemistry

journal homepage: www.elsevier.com/locate/jechem

http://www.journals.elsevier.com/journal-of-energy-chemistry/

Review

Electrocatalytic CO_2 reduction to C_2H_4: From lab to fab

Zeyu Guo [a,b,c,1], Fabao Yang [d,1], Xiaotong Li [e], Huiwen Zhu [a,b,c], Hainam Do [a,b,c], Kam Loon Fow [a,b,c], Jonathan D. Hirst [f], Tao Wu [a,b,c], Qiulin Ye [d], Yaqi Peng [d], Hao Bin Wu [e,*], Angjian Wu [d,g,*], Mengxia Xu [a,b,c,*]

[a] Department of Chemical and Environmental Engineering, and New Materials Institute, University of Nottingham Ningbo China, Ningbo 315100, Zhejiang, China
[b] Key Laboratory of Carbonaceous Waste Processing and Process Intensification of Zhejiang Province, University of Nottingham Ningbo China, Ningbo 315100, Zhejiang, China
[c] Nottingham Ningbo China Beacons of Excellence Research and Innovation Institute, University of Nottingham Ningbo China, Ningbo 315100, Zhejiang, China
[d] State Key Laboratory of Clean Energy Utilization, Department of Energy Engineering, Zhejiang University, Hangzhou 310027, Zhejiang, China
[e] Institute for Composites Science Innovation (InCSI) and State Key Laboratory of Silicon and Advanced Semiconductor Materials, School of Materials Science and Engineering, Zhejiang University, Hangzhou 310027, Zhejiang, China
[f] School of Chemistry, University of Nottingham, University Park, Nottingham NG7 2RD, UK
[g] Baima Lake Laboratory, Hangzhou 310053, Zhejiang, China

ARTICLE INFO

Article history:
Received 10 September 2023
Revised 3 November 2023
Accepted 9 November 2023
Available online 25 November 2023

Keywords:
CO_2 electroreduction reaction
Ethylene
Gas diffusion electrode
Machine learning
Density functional theory
Techno-economic analysis

ABSTRACT

The global concerns of energy crisis and climate change, primarily caused by carbon dioxide (CO_2), are of utmost importance. Recently, the electrocatalytic CO_2 reduction reaction (CO_2RR) to high value-added multi-carbon (C_{2+}) products driven by renewable electricity has emerged as a highly promising solution to alleviate energy shortages and achieve carbon neutrality. Among these C_{2+} products, ethylene (C_2H_4) holds particular importance in the petrochemical industry. Accordingly, this review aims to establish a connection between the fundamentals of electrocatalytic CO_2 reduction reaction to ethylene (CO_2RR-to-C_2H_4) in laboratory-scale research (lab) and its potential applications in industrial-level fabrication (fab). The review begins by summarizing the fundamental aspects, including the design strategies of high-performance Cu-based electrocatalysts and advanced electrolyzer devices. Subsequently, innovative and value-added techniques are presented to address the inherent challenges encountered during the implementations of CO_2RR-to-C_2H_4 in industrial scenarios. Additionally, case studies of the techno-economic analysis of the CO_2RR-to-C_2H_4 process are discussed, taking into factors such as cost-effectiveness, scalability, and market potential. The review concludes by outlining the perspectives and challenges associated with scaling up the CO_2RR-to-C_2H_4 process. The insights presented in this review are expected to make a valuable contribution in advancing the CO_2RR-to-C_2H_4 process from lab to fab.

Zeyu Guo received his B.S. degree from Anhui Normal University in 2020 and M.S. degree from University of Sheffield in 2022. Currently, he is pursuing a Ph.D. degree at the University of Nottingham Ningbo China under the supervision of Dr. Mengxia Xu. His research interests focus on the electrochemical CO_2 conversion to high value-added compounds, especially for single-atom electrocatalyst design and electrolyzer engineering.

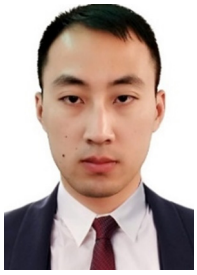

Fabao Yang received his bachelor's degree at Shandong University of Traffic and Transportation in 2014. He is currently a Ph.D. candidate at Zhejiang University under the supervision of Prof. Peng Wu. His research focuses on electrochemical conversion of CO_2 to ethylene.

* Corresponding authors at: State Key Laboratory of Clean Energy Utilization, Department of Energy Engineering, Zhejiang University, Hangzhou 310027, Zhejiang, China (Angjian Wu); Institute for Composites Science Innovation (InCSI) and State Key Laboratory of Silicon and Advanced Semiconductor Materials, School of Materials Science and Engineering, Zhejiang University, Hangzhou 310027, Zhejiang, China (Hao Bin Wu).
E-mail addresses: hbwu@zju.edu.cn (H. Bin Wu), wuaj@zju.edu.cn (A. Wu), mengxia.xu@nottingham.edu.cn (M. Xu).
[1] These authors have contributed equally to this work.

https://doi.org/10.1016/j.jechem.2023.11.019

Xiaotong Li received her Ph.D. degree from Zhejiang University in 2023. She is now working as a postdoctoral at Dalian Institute of Chemical Physics, Chinese Academy of Sciences. Her research focuses on the design and synthesis of copper-based electrocatalysts for electrochemical CO_2 reduction.

Hainam Do is an Associate Professor of Chemical Engineering at the University of Nottingham Ningbo China. He graduated with a First-Class degree in Chemical Engineering from the University of Nottingham UK, and in 2011, he received his Ph.D. in Chemistry from the same university. His current research interests revolve around energy materials, where he uses both computational and experimental tools.

Jonathan D. Hirst is a Professor of Computational Chemistry at the University of Nottingham. He was Head of School (2013—2017); his tenure saw some significant transformations under his leadership, including the building of the GSK Carbon Neutral Laboratory. In 2020, he was awarded a Royal Academy of Engineering Chair in Emerging Technology, for a 10-year project on the development and application of machine learning for green and sustainable chemistry.

Qiulin Ye is currently pursuing a Ph.D. degree at Zhejiang University under the guidance by Prof. Shengyong Lu and Dr. Angjian Wu. Her research interests focus on CO_2 electrochemical conversion to valuable products.

Hao Bin Wu is a Principal Investigator in the School of Materials Science and Engineering at Zhejiang University. He received his B.S. degree in Chemistry from Fudan University in 2010, and Ph.D. degree in Materials Science and Engineering from Nanyang Technological University under the supervision of Prof. Xiong Wen (David) Lou in 2015. After that he joined Prof. Yunfeng Lu's group at University of California, Los Angeles as a Postdoctoral Researcher. He joined Zhejiang University in July 2017. His research interests focus on electrocatalytic conversion of small molecules and high-energy-density Li/Na batteries for sustainable energy utilization. Dr. Wu has co-authored over 150 peer-reviewed articles with an H-index of 88. He was named Clarivate Analytics' Highly Cited Researcher from 2017 to 2022.

Huiwen Zhu received both his bachelor's and master's degrees from Central South University, in 2015 and 2018 respectively. He is currently a Ph.D. candidate at the University of Nottingham Ningbo China under the supervision of Prof. Tao Wu. His research focuses on the design and screening of electrocatalysts for CO_2RR by computational methods and machine learning.

Kam Loon Fow is an Assistant Professor of Chemical Engineering at University of Nottingham Ningbo China (UNNC). He received his Ph.D. degree from National University of Singapore (NUS) and worked as a Postdoctoral Fellow at KU Leuven before joining UNNC. His current research interest focuses on the synthesis and application of functionalized materials for catalysis, solid-state energy storage, 3D printing of medicine and solar cells.

Tao Wu is a Professor of Chemical Engineering at University of Nottingham Ningbo China (UNNC). He received his Ph.D. degree from University of Nottingham UK in 2007. His current research interests focus on clean energy conversion technologies, energy saving, wastewater treatment, air pollution control, etc. He serves as committee member on a number of national and regional professional bodies and is currently leading the Provincial Key Laboratory at UNNC.

Yaqi Peng is an Assistant Professor of Energy and Environmental Engineering at Zhejiang University. He received his Ph.D. degree from Zhejiang University in 2019. His research primarily concentrates on CO_2 catalytic reduction and the catalytic destruction of persistent organic pollutants (POPs).

Angjian Wu is an Associate Professor of Energy and Environmental Engineering at Zhejiang University. He received his Ph.D. degree from Zhejiang University in 2017. His current research interests focus on the development of plasma technology and electrocatalysis, including CO_2 conversion, H_2 production and nitrogen fixation.

Mengxia Xu is an Associate Professor of Energy and Environmental Engineering at the University of Nottingham Ningbo China (UNNC). He received his Ph.D. degree from the State Key Laboratory of Clean Energy Utilization, Zhejiang University in 2009 and worked as a Postdoctoral Researcher at Louisiana State University before joining UNNC in 2016. Dr. Xu's current research fields revolve around energy and environmental materials, with a particular interest on electrocatalysts for CO_2 reduction to value-added chemicals.

1. Introduction

The disruption of nature's balance caused by global warming can trigger a range of issues, including rising temperatures, sea levels, and risks to human health. Consequently, the Paris Agreement aims to curb the temperature increase to 1.5 °C by calling for appropriate measures to be taken by the international community [1,2]. In addition to global warming, the energy shortage crisis is also a matter of concern for the world. Due to its low development costs and mature conversion technologies, fossil fuels currently account for more than 80% of global primary energy [3]. However, with the world population growing rapidly, the demand for fossil energy is expected to triple in the next 30 years, resulting in an imbalance in resource supply and demand [4]. The burning of fossil fuels for almost a century has resulted in the release of large amounts of greenhouse gases, primarily carbon dioxide (CO_2). In 2022 alone, approximately 36.1 gigatons (Gt) of CO_2 gas was released into the atmosphere, posing a significant threat to ecological stability [4,5]. Therefore, there is a consensus to decarbonize the energy system and transition to green energy.

In light of global warming and the need for alternative energy sources, green energy technologies have emerged as a viable solution. As the transition to sustainable energy progresses, the efficient operation of power systems relies heavily on electrochemical energy storage [6]. The interconnectedness between various forms of energy is essential for adjusting the social energy structure and facilitating energy transformation. Electrochemistry offers an opportunity to convert electrical and chemical energy interchangeably. In the realm of renewable energy technologies, electrocatalysis plays a crucial role in the energy conversion process, particularly in fuel cells and electrolyzers. Sustainable fuel synthesis through electrocatalysis encompasses various strategies such as electrocatalytic reduction of nitrogen to ammonia [7–9], electrocatalytic conversion of light alkanes to value-added chemicals [10–12], and electrochemical CO_2 reduction reaction (CO_2RR) to hydrocarbon products [13–15].

CO_2 is an inherently stable molecule, characterized by its symmetric molecular structure. The presence of carbon in its highest oxidation state enables the acceptance of electrons, resulting in the generation of a wide range of reduction products [16]. Numerous research teams have been actively investigating various pathways for the selective conversion of CO_2 employing electrocatalysis, photocatalysis, thermocatalysis, and biocatalysis. Among these approaches, electrochemical CO_2RR has emerged as a highly promising technology for efficient conversion with a higher step and atomic economy, and lower energy costs. The advantages of CO_2RR include: (1) a relatively mild energy conversion process that does not necessitate significant additional heat input [17,18]; (2) minimal usage of chemicals, with water or wastewater as the primary byproducts [19]; (3) compact and adaptable reactors can be easily designed and scaled up as per requirement [20,21]; (4) utilization of renewable sources of electricity such as solar, tidal and geothermal energy, without further CO_2 emissions [22,23].

The pioneering work by Hori et al. shows that CO_2RR can produce a wide range of carbon products depending on the catalyst used [24]. The process of CO_2RR involves a transfer of protons and electrons and consists of multiple steps. It is responsible for converting CO_2 into valuable chemicals and fuels, specifically C_1 compounds such as carbon monoxide, methane, methanol and formic acid, as well as C_2 compounds like ethanol, ethanoic acid and ethylene (Table S1) [25–27]. Among these products, ethylene (C_2H_4) is particularly noteworthy as it serves as a primary raw material for the production of plastics, catalysts, and cleaners. The global annual production capacity of C_2H_4 currently stands at approximately 200 million metric tons, making it one of the most important organic chemicals [28–30]. The traditional methods for producing C_2H_4 involve high energy and CO_2 emissions, as they rely on steam cracking of naphtha (Europe, Asia) and natural gas-derived ethane (North America) [31]. Given the significant market size and high prices of C_2H_4, ranging from 600 to 1200 dollars per tonne (depending on region), it is a highly promising target for CO_2RR to produce C_2H_4 [23,32–34]. However, to date, there are several technical hurdles that must be addressed to produce C_2H_4 from laboratory research (lab) to industrial applications (fab) via CO_2RR. One of the main obstacles is maintaining high selectivity while achieving high reaction rates, with a desired Faradic efficiency (FE) exceeding 60%. Additionally, there is a need to reach heightened reactivity, characterized by a current density surpassing 200 mA cm^{-2}, which presents a significant challenge. Furthermore, ensuring sustained operating stability at low cell potentials is critical and requires careful consideration [35].

In the realm of electrocatalytic CO_2 reduction reaction to C_2H_4 (CO_2RR-to-C_2H_4), there exists several review articles that delve into different facets of this topic, e.g., exploring the rational design of efficient electrocatalysts and offering insights into the underlying reaction mechanisms [14,36,37]. Nevertheless, these articles fail to review and bridge the gap between fundamental research and real-world applications of CO_2RR-to-C_2H_4, neglecting to address the hidden issues in this field. In light of this, the purpose of this paper is to provide a review of the CO_2RR-to-C_2H_4 process from lab to fab. Our objectives are to primarily focus on robust cathodic materials, advanced electrolyzer devices, innovative electrolysis technologies, and the potential economic feasibility of the CO_2RR-to-C_2H_4 process. The review commences by presenting an overview of various strategies employed in the development of electrocatalysts, with a particular emphasis on rational design principles aimed at enhancing their commercial viability. Subsequently, recent research advancements related to electrolyzer devices are discussed, encompassing reactor construction, benchmarked working parameters, and the optimization of gas diffusion electrodes (GDE), thereby providing holistic insights into these critical aspects. Additionally, the review explores innovative perspectives on CO_2RR-to-C_2H_4 systems, such as electrocatalyst screening through machine learning, value-added co-electrolysis,

cascade processes, and cell stacking. Finally, the paper concludes with a techno-economic analysis (TEA) that summarizes the ecological and commercial assessments of the laboratory-derived CO_2-RR-to-C_2H_4 systems.

2. Design strategies of Cu-based electrocatalysts

The CO_2RR-to-C_2H_4 is a sophisticated process that involves multiple proton-coupled electron transfer steps, making it more intricate than hydrogen evolution reactions (HER) and other electrode reactions (see reaction network of CO_2RR in Fig. S1) [23,27,38]. This complexity poses a challenge in achieving catalysts with high-performance and uniform active sites as well as difficulties in separating the resulting products. Additionally, the lack of understanding of reaction mechanisms and active sites further complicates the optimization of electrocatalytic structures and catalytic performance. Consequently, a deeper comprehension of the structure–function relationships in electrocatalysis is imperative for modifying electrocatalyst structures and enhancing catalytic performance.

Cu-based materials are highly regarded as the most promising electrocatalyst for the CO_2RR-to-C_2H_4 process. One advantageous characteristic of Cu is its abundance, as the U.S. Geological Survey estimates a vast reserve of 210 million tons of exploited Cu resources [39]. Moreover, Cu is economically favorable, with a market price of only $9 per kilogram [40,41]. More importantly, previous studies have indicated that among metallic materials, only Cu-based materials possess the appropriate adsorption strength for *CO, an important reaction intermediate for CO_2RR [25,42–44]. For C_2H_4 electrosynthesis, the C–C coupling process is of great significance. Too weak or too strong *CO binding strength can lead to the production of C_1 compounds, thereby inhibiting the progression of C–C coupling [25,36,45–48]. Nevertheless, the current lack of commercially viable cathodic catalysts arises from the low selectivity of Cu-based electrocatalysts. Therefore, this section aims to explore the design strategies for cathodic catalysts and their structure–function relationships in the CO_2RR-to-C_2H_4 process (Table S2).

2.1. Surface functionalization

Surface functionalization is one such method that involves grafting specific groups or function-guidance molecules onto the material's surface to enhance its catalytic properties [49–51]. This approach combines the benefits of both homogeneous molecular systems and heterogeneous electrocatalysts [50,52,53], and can stabilize the microstructure of the material's surface while preserving the active sites. Additionally, surface modifiers can modulate the electronic structure of the catalyst's surface, leading to improved adsorption energy for specific reaction intermediates and enhancing the electron selectivity for the desired product (e.g., C_2H_4), while inhibiting the side reaction of HER [49,54].

The incorporation of surface functionalization has been proven to be an essential approach in stabilizing microstructures, optimizing the adsorption mode of reaction intermediates, and accelerating the mass transfer process [50,52]. Various surface additives, such as polyquinone [55], cysteamine [56–58], polypyrrole [59], polyaniline [60], and *N*-aryl-pyridinium organics [23], have been reported as effective in achieving these objectives. Previous studies have shown that organohalide salt additives in electrolytes can achieve reductive electro-dimerization process through generating organic films on the surface of Cu. For instance, *N*,*N*′-ethylene-phenanthrolinium dibromide has been observed to optimize the dimerization mechanism on the Cu surface [61]. Furthermore, the in situ electrodeposited organic film provides additional protection to the nanostructure of the Cu surface during the electrocatalytic process. Consequently, the combination of the molecular additive with the Cu electrode has resulted in a significant enhancement of C_{2+} products (FE_{C2+} > 78%, FE_{C2H4} > 45%), as illustrated in Fig. 1(a) [62]. This in situ combination strategy involving organohalide additives and polycrystalline Cu electrodes leads to the stabilization of the electrocatalyst surface with active sites. In addition, the spatial distribution of the aromatic molecules and their electronic structure play a crucial role in influencing the electrode roughness and the peripheral electron density, thereby impacting the current density and overall selectivity. Moreover, the modification of Cu with *N*-aryl-substituted tetrahydrobipyridine films and derived oligomeric films has been found to greatly enhance C_2H_4 selectivity, as demonstrated by FE_{C2H4} of 72% (Fig. 1b). Through electrodeposition, the organic film stabilizes the atop-bound *CO intermediate and promotes the coupling process of bridge-atop bound *CO, thereby facilitating the CO_2RR-to-C_2H_4 process. As a result of these properties, the *N*-aryl pyridine salt-modified Cu electrode retains high selectivity and reactivity towards C_2H_4, with long-term operating stability of up to 190 h in the membrane-electrode-assembly-based system [23].

In the context of CO_2RR, researchers have explored the use of hydrophobic polymers [54,63,64] and functional organic layers [65] to restrict water diffusion to the electrode surface, while also stabilizing electrode structure and optimizing adsorption energy. Hydrophobic layers such as 1-octadecanethiol [54,66], polytetrafluoroethylene (PTFE) [67], and poly vinylidene difluoride (PVDF) [68] have been employed to bypass HER and enhance C–C coupling. This promising design strategy involves the combination of Cu dendrites with 1-octadecanethiol to create superhydrophobic surfaces that can significantly reduce FE of HER (from 71% to 10%) while improving the selectivity of CO_2RR-to-C_2H_4 (Fig. 1c) [66]. This strategy restricts water transport and forms the triple-phase boundary (TPB), effectively trapping CO_2 gas and increasing the local CO_2 concentration on the cathode surface. Consequently, there is a notable increase in Cu-*COOH and the subsequent formation of Cu-*CO over the surface, resulting in enhanced efficiency in C–C coupling and further C_2H_4 formation [66]. Surface functionalization of electrodes with organic compounds thus presents a straightforward, controllable, and cost-effective approach for tuning the activity and selectivity of cathodic catalysts.

2.2. Morphology control

Numerous studies have confirmed the significant role that the morphology of electrocatalysts play in the heterogeneous catalytic reactions [69–71]. When developing electrocatalysts, researchers typically focus on two-dimensional scales, specifically the nanoscale and microscale, in their exploration of cathode morphology. At the nanoscale, catalyst design strategies include manipulating crystal facets, grain boundaries and defects [72–74]. Altering the nanoscale morphology can have a positive impact on the electronic structure of the catalyst surface, leading to improved utilization of active sites. Besides, alterations in material shape at microscale tend to physically alter the local microenvironment, affecting factors such as the local concentration of CO_2 and H^+, and the electrode wettability [75–78]. Material morphologies are commonly controlled by introducing defects and the exposure of different facets. Therefore, this subsection places particular emphasis on defects and crystal facets to explore their structure–function relationships during the CO_2RR-to-C_2H_4 process.

2.2.1. Defects

In metallic crystalline materials, defects serve as indicators of disorder within the periodic structure [72,79], These defects can be classified into four types based on their dimensionality: 0 D

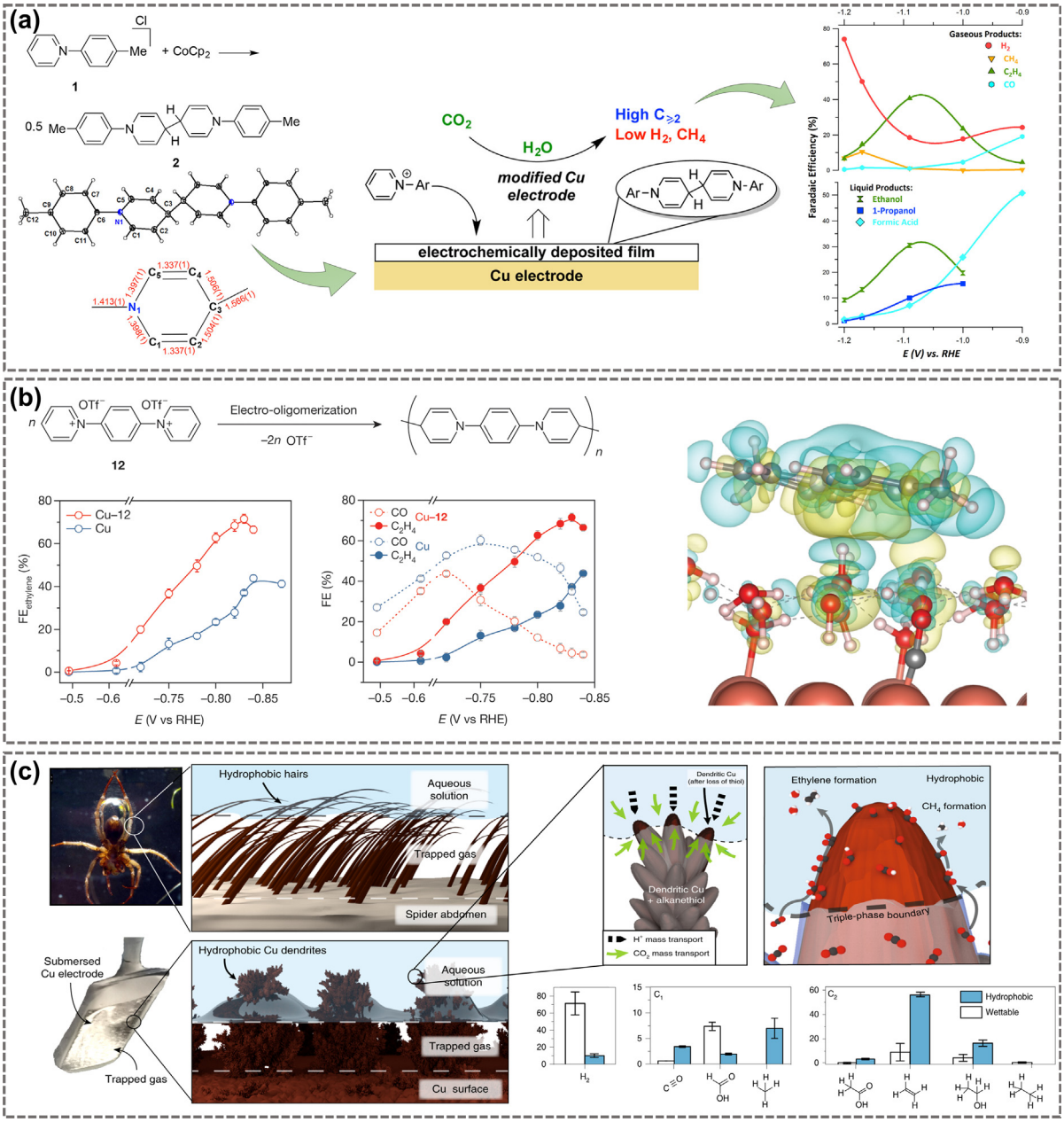

Fig. 1. (a) Synthesis, crystal structure, and selected structural parameters (Å) of surfactant. Schematic illustration of FEs towards gas products on Cu electrode depositing with N-substituted pyridinium additives. Reproduced with permission from [62]. Copyright 2022 American Chemical Society. (b) Synthesis pathway of the *N*-aryl-pyridinium organics and FE toward C_2H_4. Plots of electron density difference for the CO adsorption with one water layer and the tetrahydro-bipyridine. Reproduced with permission from [23]. Copyright 2019 Springer Nature. (c) Diagram of mass transport of reactants and product formation on the electrode surface during CO_2RR-to-C_2H_4 process by wettable and hydrophobic dendrite. FEs toward H_2, C_1 and C_2 products. Reproduced with permission from [66]. Copyright 2019 Springer Nature.

defects (point defects), 1 D defects (line defects), 2 D defects (surface defects), and 3 D defects (spatial defects) [76,80]. Controlling the introduction of defects has gained significant attention as a means of modulating the catalytic performance of catalysts. This is because defects can create active sites and mass transfer channels, as well as alter the coordination mode, local microenvironment, and electronic structure [72,79]. Various types of defects, including pores, vacancies, lattice distortions, and grain boundaries, have been intentionally introduced into Cu-based catalysts for CO_2RR-to-C_2H_4 process [76,80–82]. Research has demonstrated that effective control of defects can promote the formation of C_{2+} products in CO_2RR [80–84].

In previous studies, it has been reported that the introduction of defects during the catalyst synthesis process often leads to the formation of lattice dislocations, accompanied by changes in compression or stretching in the corresponding areas [79,82]. These nanoscale defects offer several advantages, including the optimization of active sites, enhanced conductivity, and stable adsorption sites. Specifically, defects in the metallic material serve as highly reactive sites, promoting the adsorption of intermediates on the cathodic catalyst surface. Recent research has explored the relationship between the stability of CO_2RR-to-C_2H_4 and the density of defects in catalyst materials [82]. It has been observed that the incorporation of crystal defects can enhance catalytic stability by circumventing carbon deposition, which in turn leads to the generation of CH_4 (Fig. 2a). Furthermore, the presence of defects not only prevents catalyst poisoning but also increases the coverage of *CO on the electrode surface and improves the efficiency of C–C

coupling. Notably, Cu nanoneedles with defects have demonstrated a high selectivity for C_2H_4 (FE > 62%) (Fig. 2a). Furthermore, the stability of the Cu nanoneedles during the reaction is positively correlated with the density of externally introduced crystal defects [82].

Electrochemical pulse potential treatment, as a cost-effective and straightforward method for introducing defects, offers various advantages over other methods [76,79,81]. The electrochemically treated cathode catalyst demonstrates enhanced stability within the electrochemical triple-phase boundary. Furthermore, the treatment process has the potential for industrialization by increasing the number of electrodes through parallel processing of Cu foil and expanding the electrode size to meet practical application requirements. The surface of the Cu foil after pulse potential treatment exhibits abundant defects (Fig. 2b), leading to increased adsorption of *CO on the catalyst surface, a higher roughness factor, and a higher electrochemical active surface area of the electrode (Fig. 2b, left panel). Remarkably, the cathodic catalyst treated with pulse potentials achieves a high FE_{C2H4} (>60%) at a potential of −1.0 V, and it exhibits unprecedented working stability, operating reliably in the CO_2RR-to-C_2H_4 process for over 6 months (Fig. 2b, right panel) [81]. Although the structure–function relationships between the defective Cu substrate and CO_2RR-to-C_2H_4 remain poorly understood, the electrochemical treatment strategy is intriguing due to its ability to significantly enhance electrolytic stability. Other studies have also demonstrated the performance-enhancing effects of introducing defects in Cu-based nanomaterials for CO_2RR [76,80,84]. However, there is limited research on controlling the number and distribution of defects. Thus, it is imperative to analyse the structure–function relationships between defects and catalytic performance to develop defect engineering strategies.

2.2.2. Crystal facets

The process of modifying the exposed facets of catalysts, commonly referred to as "facet control", is widely recognized for its effectiveness in altering catalytic performance for various chemical reactions [73,74]. This technique involves selectively tuning the exposed crystal facets of catalysts by regulating nucleation rates or employing capping agents. Recent studies have revealed that different facets of Cu-based catalysts possess distinct atom arrangements and surface energy, which significantly influence the activity and selectivity of CO_2RR [77,78,85,86]. For instance, Cu(111) facets promote CH_4 production, while Cu(100) facets are known for *CO dimerization, resulting in C_2H_4 formation during the CO_2RR process. Cu metal possesses a thermodynamically stable face-centered cubic crystalline phase. By employing kinetic and thermodynamic control, Cu nanocrystals (NCs) with various morphologies, such as 0-dimensional nanoparticles, 1-dimensional nanowires, and 2-dimensional nanosheets, can be synthesized. Furthermore, it is possible to achieve controlled design of Cu polyhedra that expose the desired crystal facets [77,87].

To examine the correlation between the structure and function of Cu nanocatalysts, Gregorio et al. synthesized catalysts in various shapes, such as spherical, cubic, and octahedral shapes, which exposed distinct Cu facets (Fig. 3a) [77]. The CO_2RR performance of different Cu nanocatalysts was subsequently assessed using a flow-cell at ampere-level current densities in a 1 M KOH solution. The results indicate that the cubic Cu NCs with exposed (100) facets display an improved C_2H_4 selectivity (up to ∼57%) and a mass activity of 700 mA mg^{-1}. Conversely, the octahedral Cu NCs with exposed (111) facets exhibit an enhanced methane selectivity (up to ∼51%) with a mass activity of 1.45 A mg^{-1} (Fig. 3b) [77]. Hence, an increase in the proportion of Cu(100) facets among the exposed facets proves effective in promoting C_2H_4 formation. To achieve this, Li et al. designed a Cu NC with a higher ratio of Cu (100) facets to Cu(111) facets by selectively coating the Cu(111) surface with an ultrathin Al_2O_3 layer (Fig. 3c), resulting in a higher FE_{C2H4} of 60.4%. The FE ratio of C_2H_4 to CH_4 for Al_2O_3-coated Cu NCs is 22 times greater than that of pristine Cu NCs (Fig. 3d) [78]. Notably, Cu catalyst synthesized via electrodeposition under a CO_2 atmosphere (Cu-CO_2) exhibits a 70% increase in the ratio of Cu (100) facets to total facets area compared to that electrodeposited in a N_2 atmosphere. Consequently, the Cu-CO_2 catalyst achieved a high FE_{C2H4} of 65% (Fig. 3e) [75].

2.3. Alloy system construction

The utilization of nanostructured alloys has proven effective in catalysing heterogeneous electrocatalytic reactions. This efficacy can be attributed to various factors, such as the alloy's capacity to enhance product selectivity and lower the overall energy barrier of the reaction [88–91]. This improved performance is a result of the elemental bifunctionality, electronic structure, and geometric strain present in the alloy material [88,90,92]. Previous studies have focused on investigating Pt alloys with transition metals like Mn, Ti, V, and Mo for the oxygen reduction reaction (ORR) dating back to the 1980 s [93–95]. Additionally, within the realm of CO_2-RR research, the incorporation of other elements into Cu-based catalysts has proven to be advantageous in attaining enhanced performance. This approach can significantly alter the surface binding energy and optimize the adsorption mode of intermediates on the electrode surface through the single-atom alloy construction, strain regulation, among others [96,97].

In recent years, researchers have utilized Cu-based poly-alloy catalysts with confined nanostructures in their research on CO_2RR [88,92,94,95]. These alloy catalysts have been the subject of investigation in order to understand the relationship between their physical characteristics, such as mixture patterns (disordered, ordered, and phase-separated atomic mode), and their electrocatalytic performance. Experimental findings using Cu-Pd catalysts indicate that bimetallic alloy catalysts with disordered atomic arrangements have a relatively high HER selectivity. Interestingly, alloys with an ordered atomic arrangement (Cu:Pd = 1:1) displayed the highest selectivity (FE > 80%) for C_1. Furthermore, the phase-separated alloy material (Cu:Pd = 1:1), which consists of three separate phases (face centered cubic type Cu and Cu_2O, and face centered cubic type Pd), demonstrated the highest total current density and the highest selectivity for C_2H_4 (370 mA cm^{-2}, FE > 45%) (Fig. 4a) [98]. These experimental results indicate that the geometric arrangement of the materials can influence the selectivity of CO_2RR products. This advancement in understanding the relationship between the structure and function of CO_2RR-to-C_2H_4 is crucial for the engineering of alloy catalyst.

The process of alloying has been found to facilitate the localized redistribution of electrons in pure Cu, resulting in changes in the distribution of CO_2RR products. When comparing Cu-Sb alloy to pure Cu, the electronic configuration is optimized, charge transfer resistance is reduced, and the electrochemical surface area is increased. Additionally, doping of Ce^{3+} in Cu-Ce alloys leads to the creation of oxygen vacancies near Ce atoms, which in turn modifies the electronic state of Cu atoms. This modification of the electronic structure can be utilized to enhance the electrocatalytic properties of the metal active sites, ultimately leading to a more efficient CO_2RR-to-C_2H_4 process. Experimental results indicate that the inclusion of non-precious metal elements in the alloy catalysts Cu_{10}-Sb_1 and Cu-Ce resulted in C_2H_4 Faradaic efficiencies of 49.7% and 53%, respectively, when tested in 0.1 M KCl and 1 M KOH solutions, as shown in Fig. 4(b and c) [99,100].

The utilization of tandem catalysts consisting of Cu and noble metals like Au, Ag, and Pd effectively enhances the CO_2RR-to-C_2H_4 process. The inclusion of Ag or Au in the Cu-Au, Cu-Ag, or Cu-Au-Ag alloy systems increases the probability of C–C coupling

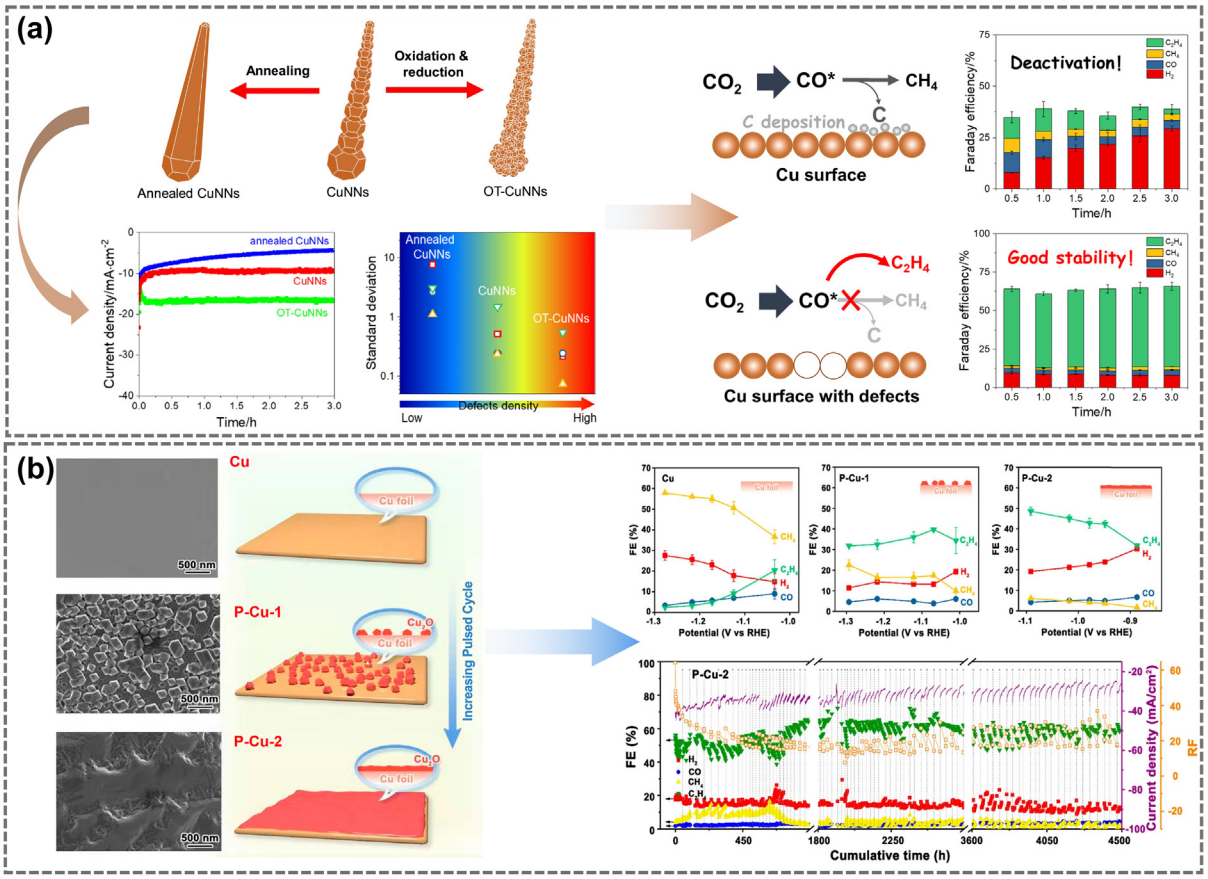

Fig. 2. (a) Schematic illustration of treatments to eliminate or increase the number of defects in Cu nanoneedles. Proposed mechanism and obtained FEs toward gas products for different Cu electrodes. Reproduced with permission from [82]. Copyright 2019 Elsevier. (b) Schematic diagram of electrochemical pulsed potential treatment. FEs of gaseous products on P-Cu-2 (pulsed synthesis with 900 cycles) and comparison of C_2H_4/CH_4 ratios and roughness factor (RF) for as-prepared catalysts. Reproduced with permission from [81]. Copyright 2022 American Chemical Society.

on the adjacent Cu, resulting in a higher local concentration of *CO. An example of this is the electrodeposited Cu-Ag catalyst, which demonstrates FE_{C2H4} of 60% at low potentials (−0.7 V vs RHE) and a total current density of approximately 300 mA cm^{-2} (Fig. 4d) [101]. Similarly, the polynary Cu-Au/Ag nano-framework materials exhibit significant selectivity for C_2H_4, with 69% ± 5% and 77% ± 2% in H-cell and flow-cell setups, respectively (Fig. 4e) [102]. Furthermore, mechanistic investigations suggest that Cu with a positive charged and a highly distorted lattice effectively lowers the energy barrier for the rate-determining step. This is due to the strong lattice mismatches and electronic interactions between the Ag/Au substrate and the Cu complement. Additionally, Ag-Cu Janus nanostructures with (100) facets, as depicted in Fig. 4(f), exhibit superior CO_2RR performance for C_{2+} products, particularly with FE_{C2H4} of 54%. This can be attributed to their optimized electronic structure and the tandem electrocatalytic reduction of CO_2 [103].

2.4. Oxidation state regulation

The oxidation state is defined as "the degree of oxidation of an atom based on electron counting" [104]. Determination of the oxidation states can reveal the chemical state of the elements and rationalize the design of electrocatalysts. By regulating the oxidation state, the number of valence electrons can be modified, leading to changes in electron distribution. For transition metal atoms, adjusting the oxidation state can alter the arrangement of empty *d*-orbitals and unpaired d-electrons, which is crucial for electron transfer to reactants [46]. In the process of CO_2RR-to-C_2H_4, controlling the oxidation state can facilitate the activation of CO_2 molecules, the adsorption of reaction intermediates, and the promotion of C–C coupling, thereby lowering the energy barrier of the overall reaction [46,105]. It has been reported that $Cu^{\delta+}$ ($0 < \delta + < 1$) plays a critical role in directing the CO_2RR pathway towards efficient C_{2+} formation. However, $Cu^{\delta+}$ species experience in situ self-reduction during long-term electrolysis, especially under industrial current densities [106,107]. Therefore, addressing these issues and optimizing the oxidation state of Cu-based electrodes to achieve high selectivity and stable operation of CO_2RR-to-C_2H_4 has become a priority [107–109]. Hence, this subsection aims to examine the impact of modifying the oxidation state of the cathode materials on CO_2RR-to-C_2H_4.

Plasma treatment techniques are extensively employed in the generation of oxide layers on metal and alloy surfaces [110]. In the realm of electrocatalyst design, the strategy of plasma-mediated oxidation state adjustment has been utilized to produce Cu-based catalysts with a surface oxide layer and a low coordination active site, specifically Cu^+ species. The cathode material that undergoes plasma activation contains a substantial amount of active Cu^+ species on its surface, which enhances the production of C_2H_4 and reduces the onset potential. Experimental results have shown that the plasma-activated oxide-derived Cu (OD-Cu) catalyst effectively suppresses CH_4 production, resulting in a 60% selectivity for C_2H_4 at a lower overpotential of CO_2 reduction (−0.9 V vs. RHE) [42,105]. Additionally, it has been observed that subjecting the same plasma-mediated Cu-based material to H_2 plasma

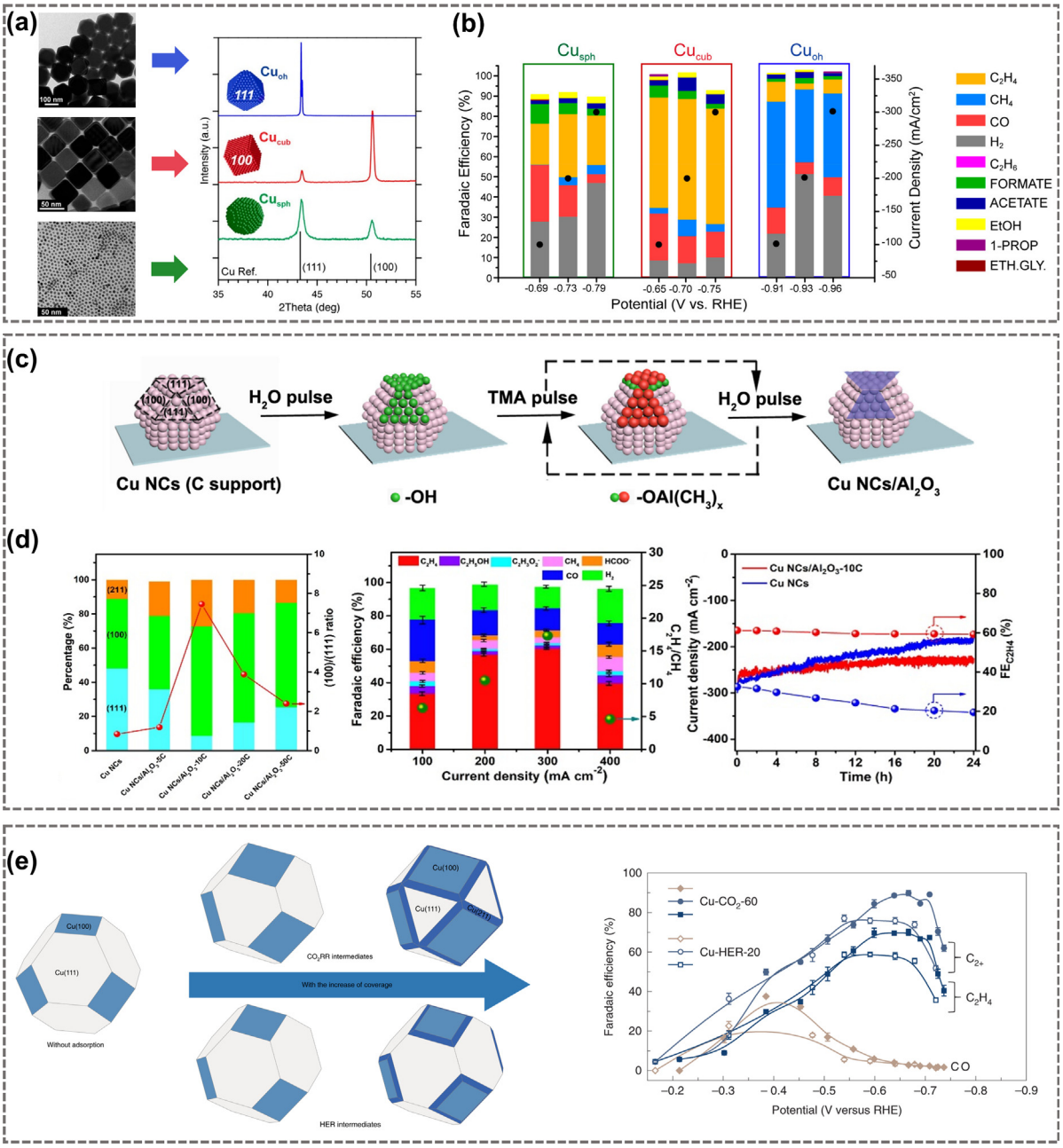

Fig. 3. (a) Morphology and XRD patterns of Cu spheres (Cu_{sph}), Cu cubes (Cu_{cub}) and Cu octahedra (Cu_{oh}) with different facets, and (b) the product distribution of CO_2RR over three Cu catalysts with different facets exposure. Reproduced with permission from [77]. Copyright 2020 American Chemical Society. (c) Schematic diagram of selectively covering Cu(111) surface of Cu nanocrystals (NCs) with ultrathin Al_2O_3 layer. (d) The product distribution of CO_2RR over Al_2O_3 selectively covered Cu NCs catalyst. Reproduced with permission from [78]. Copyright 2021 John Wiley and Sons, Inc. (e) CO_2 reduction intermediates adsorption enhanced the exposure of Cu(100) and selectivity to C_2H_4 and C_{2+} products. Reproduced with permission from [75]. Copyright 2019 Springer Nature.

reduces the quantity of Cu^+ species on the surface. Despite retaining similar surface roughness, the plasma-mediated Cu-based material with a higher concentration of Cu^+ species on the surface exhibits superior performance during the CO_2RR-to-C_2H_4 process, thereby highlighting the significance of plasma-mediated Cu^+ as the active species (Fig. 5a) [110].

Furthermore, as an alternative to plasma-mediated strategies, the solvent thermal synthesis technique has been employed to produce an OD-Cu catalyst. This catalyst, enriched with $Cu_2^+Cu_2^{2+}O_3$, exhibits a paramelaconite-like nature characterized by a mixed valence state of Cu^+ and Cu^{2+}. This unique feature allows for a diverse range of valences on the surface active sites of the initial template. Consequently, the catalyst demonstrates an exceptional selectivity for hydrocarbon products along with enhanced stability. Notably, this catalyst demonstrates a high current density of 400 mA cm^{-2} and a stable FE of 43% for C_2H_4 in a flow-cell. When compared to the OD-Cu catalyst treated with plasma, the solvent heat-treated catalyst showcases remarkable long-term operating stability, lasting for 24 h at current density of 200 mA cm^{-2} (Fig. 5b) [48]. Additionally, various Cu-based catalysts with different oxidation levels have been prepared using electrochemical treatments such as as-prepared, cyclic voltammetry (CV), and electrodeposition. These treatments lead to OD-Cu catalysts dominated by Cu (0), coexistence of Cu(I) and Cu(0) states, and Cu(I), respectively. Data gathered from CO_2RR experiments suggest that among the three OD-Cu catalysts, the CV-treated Cu electrode, containing both

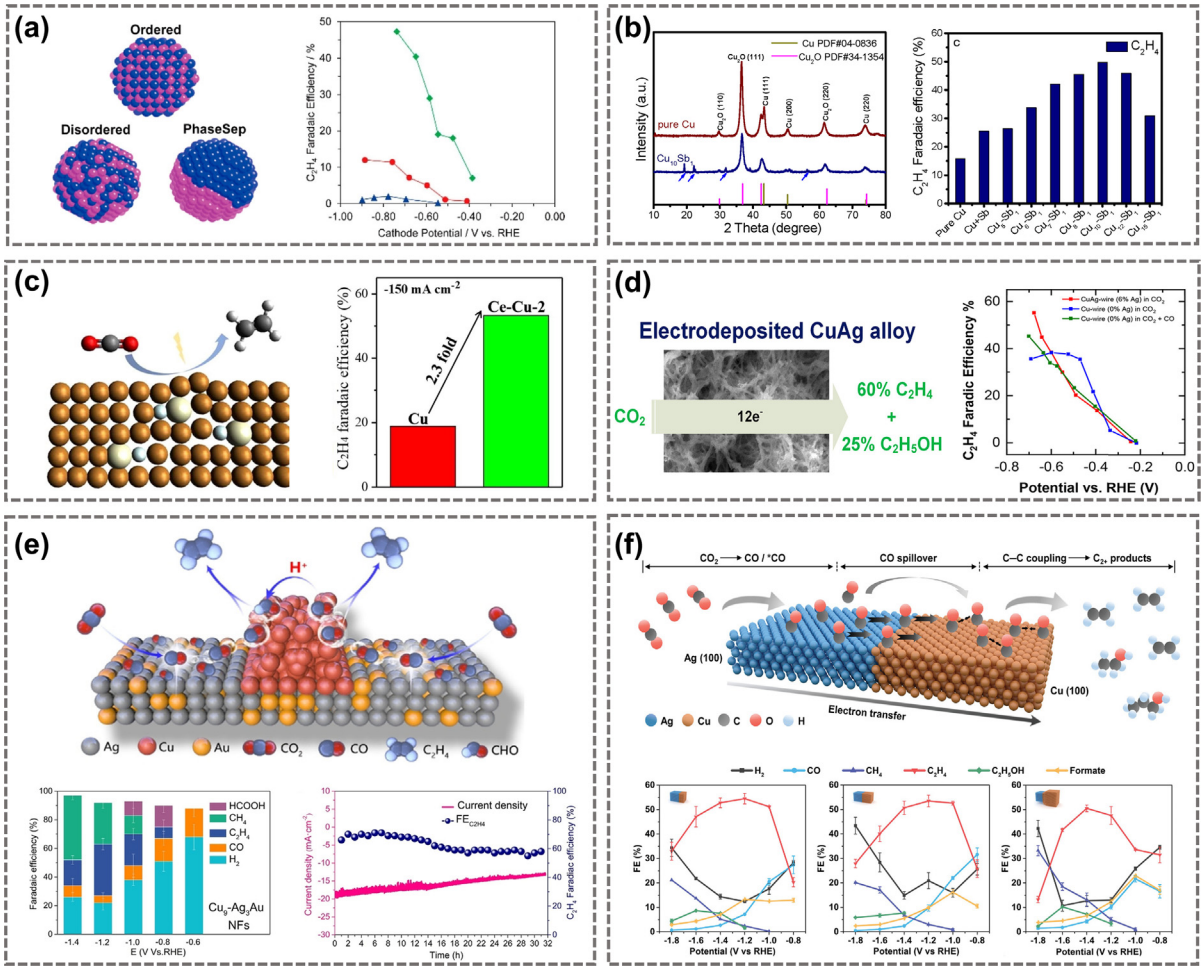

Fig. 4. (a) Schematic illustration of prepared Cu-Pd nanoalloys with different structures. FE_{C2H4} for bimetallic Cu-Pd catalysts with different mixing patterns: ordered, disordered, and phase-separated. Reproduced with permission from [98]. Copyright 2017 American Chemical Society. (b) XRD patterns of the Cu-Sb catalysts and corresponding CO_2RR-to-C_2H_4 selectivity. Reproduced with permission from [99]. Copyright 2020 Elsevier. (c) Model of Cu nanoparticles doped with Ce. Comparison of FE_{C2H4} for obtained Cu and Ce-Cu-2 catalyst. Reproduced with permission from [100]. Copyright 2021 Elsevier. (d) Schematic diagram of a porous Cu-Ag alloy and CO_2RR-to-C_2H_4 performance. FE_{C2H4} from Cu wire and CuAg wire in different gas feeding. Reproduced with permission from [101]. Copyright 2018 American Chemical Society. (e) General mechanistic overview, selectivity, and stability of C_2H_4 production of Cu_3-Ag_3Au catalyst. Reproduced with permission from [102]. Copyright 2020 John Wiley and Sons, Inc. (f) Illustration of a plausible CO_2RR mechanism on Ag_{65}–Cu_{35} JNS-100 (Ag–Cu Janus nanostructures with 100 facets) and FEs toward different products. Reproduced with permission from [103]. Copyright 2022 John Wiley and Sons, Inc.

Cu(I) and Cu(0) regions, exhibit the highest C_2H_4 generation with FE exceeding 40% (Fig. 5c).

The application of in situ surface-enhanced infrared absorption spectroscopy (SEIRAS) has facilitated the identification of both atop-bound and bridge-bound *CO intermediates during CO_2RR on a CV- treated Cu electrode (Fig. 5d) [111]. This treatment has been shown to enhance the dimerization of *CO and improve the selectivity of C_2H_4 product. This study demonstrates that the design of Cu valence states is an effective strategy for investigating their impact on the selectivity of C_2H_4 product in CO_2RR. Xia and co-workers have developed Cu-based catalysts with different oxidation levels by adjusting the amounts of reducing agents. The catalysts with the optimal oxidation level are capable of inhibiting the hydrogenation reaction (formation of CH_4) and promoting C–C coupling, resulting in FE_{C2H4} of 53% (Fig. 5e) [109]. Additionally, Cu-based catalysts with varying valence states (Cu-pC, Cu_2O-pC, and Cu_2O/Cu-pC, where pC denotes porous carbon) have been obtained by manipulating the gas type and oxygen concentration during the annealing process. Among these Cu-based materials with different oxidation states, Cu_2O/CuO-pC displays the highest selectivity for C_2H_4, achieving FE of 65.1% at current densities up to 578 mA cm^{-2} in a 1 M KOH electrolyte (Fig. 5f) [45,108].

3. Design strategies of robust CO_2RR-to-C_2H_4 devices

3.1. CO_2RR electrolyzer devices

3.1.1. Overview

Electrolyzers encompass both solid oxide electrolyzers operating at high temperatures (above 600 °C) and low-temperature (room-temperature) electrolyzers. While significant progress has been made in the electrolysis of CO_2 into CO using solid oxide electrolyzers, the high-temperature conditions are not conducive to the formation of C_2 compounds through C–C coupling [112]. Consequently, the production of C_2H_4 and other compounds primarily takes place in room-temperature CO_2 electrolysis. Therefore, this section focuses on the production of C_2H_4 in a room-temperature electrochemical system [113,114]. To achieve the production of C_2H_4 at room-temperature, three primary electrochemical systems are employed: the H-type cell, flow-cell, and membrane electrode assembly (MEA) cell, as depicted in Fig. S2. These electrochemical systems offer distinct approaches for synthesizing C_2H_4, each possessing unique advantages and considerations. The H-cell

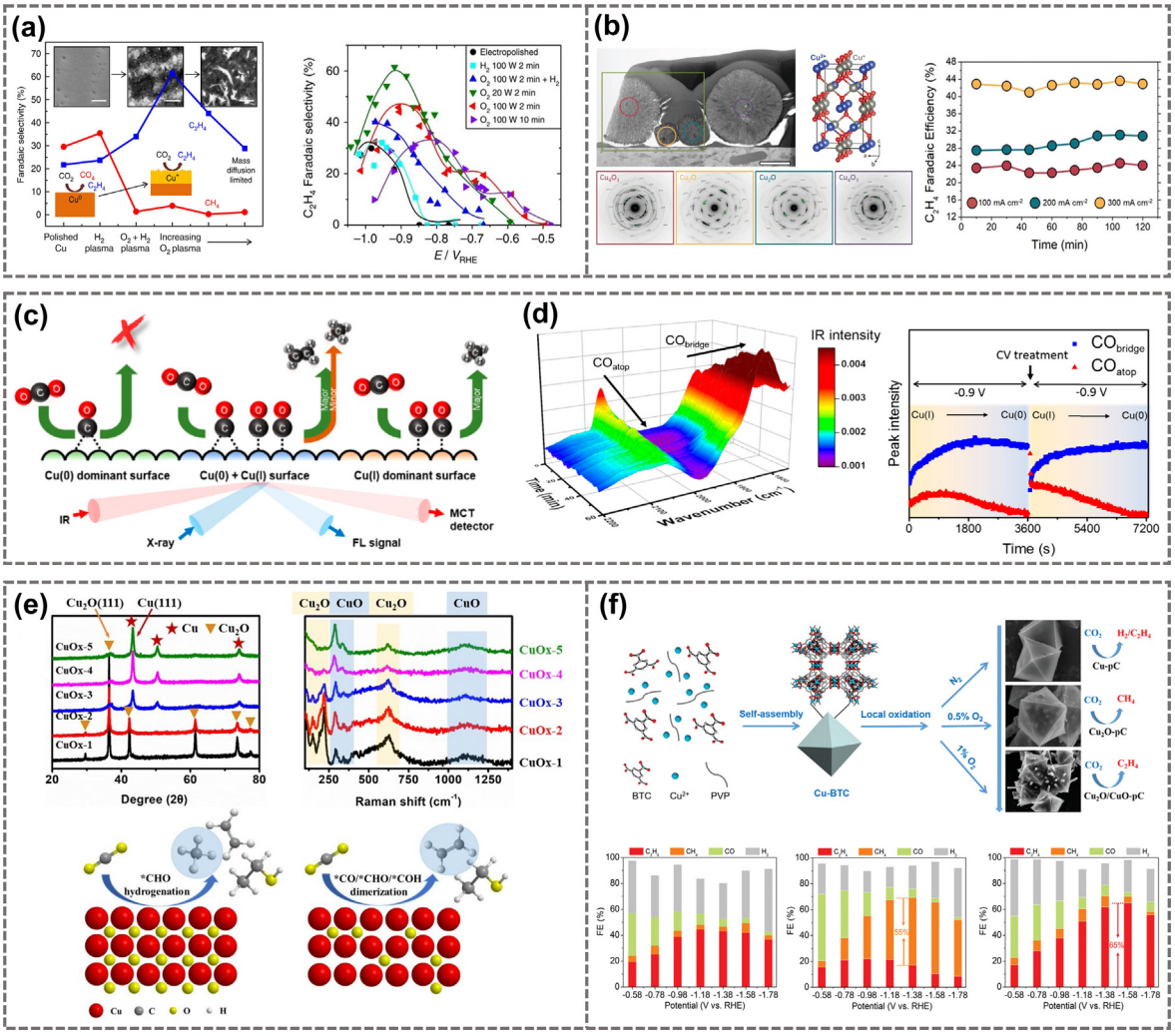

Fig. 5. (a) From left to right, the SEM images of the low surface area H_2 plasma-treated Cu foil, the O_2 20 W 2 min plasma-treated Cu foil with optimal C_2H_4 selectivity, and the O_2 100 W 10 min oxidized sample after the reaction. FE_{C2H4} of as-prepared Cu foil. Reproduced with permission from [110]. Copyright 2016, The Authors. (b) Paramelaconite crystal structure, XRD pattern and FE_{C2H4} of the synthesized Cu_4O_3-rich catalyst. Reproduced with permission from [48]. Copyright 2019 John Wiley and Sons, Inc. (c) Schematic illustration of the CO_2RR-to-C_2H_4 on the three Cu surfaces with different amounts of Cu(I) and Cu(0) states. (d) In situ SEIRAS of CV-treated electrode and time-dependent CO_{bridge} and CO_{atop}-associated peak intensities. Reproduced with permission from [111]. Copyright 2020 American Chemical Society. (e) XRD pattern and Raman spectra of CuO_x catalysts (top part). Schematic illustration of the CO_2RR-to-C_2H_4 on high/low oxidation CuO_x catalysts (bottom part). Reproduced with permission from [109]. Copyright 2022 American Chemical Society. (f) Schematic flowchart of the fabrication of catalysts with adjustable morphology. FEs of different products for Cu-pC, Cu_2O-pC, and Cu_2O/CuO-pC, respectively (bottom part, from left to right). Reproduced with permission from [108]. Copyright 2022 John Wiley and Sons, Inc.

configuration utilizes a liquid electrolyte, while the flow-cell operates with a continuous flow of electrolyte. On the other hand, the MEA system incorporates a membrane electrode assembly, which facilitates selective ion transport and catalytic reactions [115].

3.1.2. H-cell

In the H-cell configuration (Fig. S2a), the integration of the cathode and anode compartments within the electrolyte are seamless. The ion-exchange membrane plays a crucial role as a selective barrier, effectively separating the distinct reaction environments of the cathode and anode. However, achieving high current densities exceeding 200 mA cm^{-2} in H-cells is a significant challenge primarily due to diffusion limitations. The sluggish diffusion characteristics, especially the relatively low diffusion coefficient of CO_2 ($t_{CO2} = 1.94 \times 10^{-3}$ mm^2 s^{-1} at 25 °C), restrict the mass transfer rate during the CO_2RR process [114]. Consequently, these diffusion limitations hinder the attainment of higher current densities in the CO_2RR process [113,114]. Another limitation of the H-cell configuration is its incompatibility with alkaline electrolytes, as hydroxide ions readily react with dissolved carbon dioxide, resulting in the formation of carbonates [34,116,117]. Furthermore, the use of non-alkaline electrolytes exacerbates the occurrence of ohmic overpotential [118].

3.1.3. Flow-Cell

Liquid electrolyte flow-cells are the most extensively studied reactors in the CO_2RR process. This electrolyzer can achieve industrial currents readily and potentials can be monitored by inserting reference electrodes for CO_2RR fundamental research (Fig. S2b) [119,120]. The flow-cell configuration offers a viable solution to address the challenges associated with the liquid-based systems. Instead of relying on liquid, the flow-cell diffuses the gas directly onto the electrode surface [121–124]. In this setup, gaseous CO_2 is fed directly into the interface between the catalyst and the electrolyte, promoting efficient mass transfer of CO_2 to the catalyst layer. This design enables swift diffusion of CO_2, thereby enhancing the overall performance of the flow-cell electrolyzer [125,126]. The use of gas diffusion electrode (GDE) in flow-cells introduces new

design concepts and operating principles in the field of CO_2 abatement, and also improves the feasibility of gas-fed reactors for commercial applications [127,128]. As reported, a gas-fed flow-cell with an alkaline electrolyte (10 M KOH) can operate at a constant voltage of −0.55 V (vs RHE) for 150 h, producing C_2H_4. Furthermore, increasing the electrolyte's concentration enhances conductivity, improves reaction kinetics, and enables a current density of approximately 200 mA cm^{-2} to be achieved at an overpotential of less than 0.7 V [118].

3.1.4. MEA

The MEA cell, depicted in Fig. S2(c), is a significant advancement in gas-fed flow-cell technology. This cell configuration eliminates the need for cathode flowing electrolyte by directly placing the cathode GDE in close proximity to the ion exchange membrane [20,129]. Referred to as the zero-gap design structure, this arrangement offers a distinct advantage by greatly enhancing the rate of the CO_2RR. However, the use of MEA results in the reaction of CO_2 with the strong alkaline electrolyte, leading to the formation of (bi)carbonates and the precipitation of salts on the GDE and ion exchange membranes. This situation can cause a decrease in the conductivity of the entire system [130]. Additionally, the liquid product can be diluted into the bulk electrolyte, thereby increasing downstream separation costs. Urgent issues to be addressed include catholyte stability, ohmic loss of electrolyte, consumption of CO_2 due to its reaction with the electrolyte, catalyst contamination caused by electrolyte impurities, and flooding of the GDE. Therefore, the design of an electrolytic cell capable of overcoming these challenges is of utmost importance for the industrial application of CO_2RR [131].

3.2. Benchmarked working parameters

After describing the three types of electrolyzers, it becomes crucial to present benchmarked working parameters. This is necessary to ensure that the cost associated with deploying the CO_2RR electrolyzer remains within acceptable limits over its operational lifespan [132–136]. Firstly, in the context of commercial CO_2RR-to-C_2H_4, it is imperative to achieve current densities higher than 200 mA cm^{-2} [45,132,137–141]. Additionally, to optimize the selectivity of C_2H_4 production and minimize expenses associated with product separation, maintaining FE of over 60% for large-scale production is essential [31,32,117,138]. In addition, it is crucial to consider the energy efficiency (EE) and CO_2 single-pass conversion (SPC) efficiency. Tables S3 and S4 in the Supporting Information offer comprehensive comparisons of reported EE [23,32,117,142–145] and SPC [146–153] of C_2H_4 electrolysis in various electrolyzer setup. In the progressive advancement and implementation of renewable electricity sources, achieving an EE exceeding 50% in the commercial CO_2RR-to-C_2H_4 is crucial [31,154]. Jiao's research group has discovered that the SPC efficiency of CO_2RR-to-CO is typically restricted to approximately 43% due to the constraint imposed by carbonate precipitation, which consumes around 55% of the CO_2 feed [155]. When scaling up CO_2RR-to-C_2H_4, it is imperative to acknowledge the limitations imposed by SPC efficiency. Finally, the device's durability must meet commercial requirement, with a stable operation duration of at least 100 h under industrial-level current density [32]. These criteria are of utmost importance to ensure that the overall cost remains economically viable and acceptable [23,31]. Currently, only flow-cell and MEA electrolyzers can meet industrial standards, indicating their superior performance and suitability for industrial-scale applications.

Through experiments conducted in both flow-cell and MEA setups for a duration of approximately 120 minutes, the obtained data reveal notable findings. Specifically, it is observed that the MEA exhibits the lowest and most stable voltage of −4 V (Fig. 6a). Conversely, the neutral and alkaline flow-cells demonstrate comparatively less stability, with higher fluctuation voltages reaching approximately −5 V. Furthermore, Fig. 6(b) illustrates that the MEA achieves a remarkable selectivity of C_{2+} products, with the FE_{C2H4} reaching nearly 50%, surpassing the selectivity of the other two cells [32].

3.3. Optimization strategies of GDE

3.3.1. Overview of GDE

The development of GDEs has been crucial in overcoming the limitations imposed by mass transfer. These electrodes enable the direct introduction of gaseous carbon dioxide into the catalyst located on the porous cathode, thereby effectively addressing the aforementioned constraints. In the context of flow-cells and MEA cells, GDEs play a ubiquitous role and consists of three fundamental components: a porous catalyst layer, a gas diffusion layer (GDL) that serves as both an electrically conductive and porous scaffold, and a gas flow field designed to facilitate gas transport and provide mechanical reinforcement [156]. Fig. S3 illustrates the basic structure of GDE in an CO_2RR electrolyzer. The catalyst in contact with the electrolyte is deposited on the porous GDL. The GDE can be conceptualized as an electrode structure with porosity that hosts the catalyst material. The GDL, a porous braided layer, supports the catalyst and serves as the channel for CO_2 to reach the catalyst surface [120,128,157]. During the CO_2RR process, CO_2 penetrates the hydrophobic porous layer, diffusing onto the catalyst surface. Analysis using reaction–diffusion models and experimental results indicates that an abrupt reaction interface can reduce the interaction between CO_2 and alkaline electrolyte [158]. The GDE plays a pivotal role in modulating the electrocatalytic performance by influencing the transport phenomena of CO_2, water, and hydroxide species [157]. It is important to design the GDE carefully to ensure efficient transportation of these crucial materials, as improper design can lead to adverse consequences such as flooding and the deposition of carbonates.

3.3.2. Failure of GDE

The failures observed in GDEs are primarily attributed to the precipitation of carbonates, which subsequently triggers flooding, enhanced HER, and other associated complications [159–161]. The generation of hydroxide ions (OH^-) at the interface between the electrolyte and electrode causes a local increase in pH value. Simultaneously, CO_2 reacts with OH^- to form (bi)carbonates at this interface. The gradual accumulation and deposition of (bi)carbonates on GDE surfaces and CO_2 flow paths result in contamination of the electrolyte and subsequent failure of the GDE [162,163]. Additionally, the formation of (bi)carbonates can draw the electrolyte into the GDE, leading to flooding issues. The occurrence of flooding within an electrolyzer is closely linked to changes in the concentration of CO_2 and H_2O in the microenvironment. For instance, flooding issues can reduce the concentration of CO_2 in the local microenvironment, thereby hindering the efficiency and selectivity of the CO_2RR-to-C_2H_4 process [61,155]. In cases where the cathode experiences limited CO_2 availability, the HER surpasses CO_2RR in terms of reaction rates [164]. Moreover, excessive water will impede the entry of CO_2 into the electrode, leading to an increase in the number of crossover sites [165].

To address the issue of (bi)carbonate accumulation and deposition on GDE, various strategies have been explored to prevent GDE failure. Experimental studies (catalyst thickness: 25–1000 nm, electrolyte concentration: 1–7 M KOH) have shown that GDEs with a common structure tend to lose their hydrophobic properties and

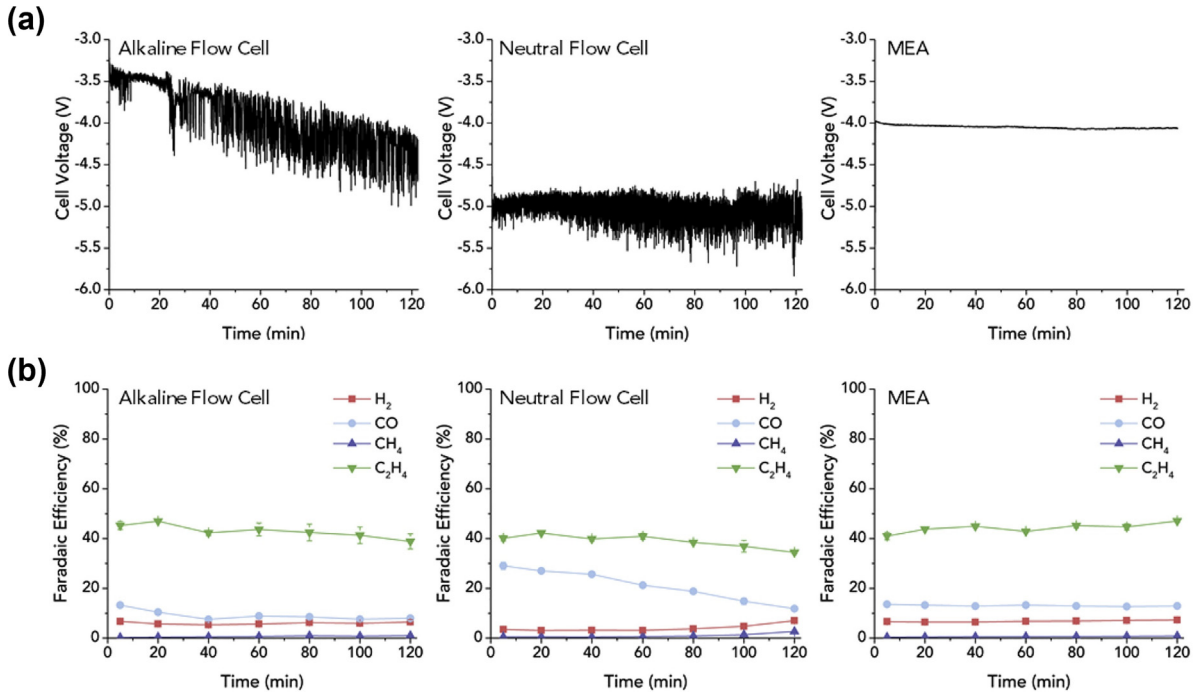

Fig. 6. Stability of the cell voltage (a) and gas products (b) for 120 min in alkaline flow-cell, neutral flow-cell, and MEA with an applied current of 750 mA (150 mA cm^{-2}). Reproduced with permission from [32]. Copyright 2019 Elsevier.

experience performance degradation within one hour of continuous operation of CO_2RR [118,134]. Fig. 7(a and b) illustrate two potential approaches to enhance the stability of the electrolytic cell.

The first approach involves increasing the temperature of the CO_2 inlet, which leads to a continuous supply of water vapor into the cell. When the inlet temperature of CO_2 is at 60 °C (Fig. 7b), the FE_{CO} can be maintained at above 80%. However, when the temperature is raised further to 85 °C, a gradual decline of FE_{CO} is observed due to the precipitation of K_2CO_3 (Fig. 7a). The second approach involves periodically rinsing the battery with liquid water. A 10-second rinse with deionized water at the start of each hour can repair the cell stack and restore the current to its original value (~250–275 mA cm^{-2}). The FE of CO throughout the electrolysis process is approximately 85%. Comparing the current values at the end and beginning of each method, no significant decrease is observed over an 8-h period, indicating the absence of irreversible degradation. Both approaches effectively prevent the accumulation of K_2CO_3 precipitates, and periodic rinsing of the electrolytic cell with deionized water reduces carbonate precipitation and flooding while increasing the current density [118,134].

Although there are methods such as increasing the temperature of the CO_2 feed or periodically flushing the GDE can partially mitigate carbonate precipitation and GDE collapse, these approaches are not suitable for large-scale implementation due to their high cost and complex operation. Recently, the use of solid polymer electrolytes instead of alkaline electrolytes has emerged as a promising strategy to avoid carbonate precipitation. In this MEA-type system, only CO_2 and pure water are supplied for co-electrolysis, preventing salt precipitation in principle (Fig. 7c) [144,166,167]. Zhuang's research group reported the first pure water MEA for CO_2RR-to-CO in 2019, reaching an industrial-scale current density of 500 mA cm^{-2} [166]. Building on this success, the team further achieved high-current–density of CO_2/pure water co-electrolysis toward C_2H_4 formation by introducing quaternary ammonia poly(ether ether ketone) (QAPEEK) into Cu-based GDE. QAPEEK, serving as a polymer electrolyte, not only possesses ionic conductivity but also facilitates the activation of CO_2 molecules. This electrolyzer, which solely consumes CO_2 and pure water, demonstrates a total current density of 1.0 A cm^{-2} at cell voltages as low as 3.73 V. Moreover, efficient CO_2RR-to-C_2H_4 at partial current densities of 420 mA cm^{-2} was achieved at applied voltages up to 3.54 V (Fig. 7d) [144].

3.3.3. Confined triple-phase boundary of GDE

The three-dimensional structure of GDE creates a triple-phase boundary (TPB) consisting of gas, liquid, and solid, which is crucial for optimizing the mass transfer process in CO_2RR. This unique characteristic of GDE allows for enhanced catalytic performance, surpassing what is achievable with planar catalyst surfaces, resulting in increased conversion and energy efficiency [124,168–170]. In comparison to the conventional two-chamber H-cell, where the contact between liquid and solid is limited, GDE facilitates the formation of a gas–liquid-solid TPB, further optimizing the mass transfer process for CO_2RR. In summary, the design of GDE for high CO_2RR performance is based on three factors: the presence of abundant TPB, excellent and long-lasting electrical conductivity, and optimized dissociation and diffusion of product molecules [124,152]. An illustrative example of this design approach is the graphite/carbon NPs/Cu/PTFE electrode, which is capable of tolerating bases by optimizing CO_2 diffusion into the catalytic site. This electrode configuration, consisting of multiple stacked catalyst layers, enables the production of C_2H_4 under strong basic conditions at 7 M KOH, with a consistent and high FE of 70% (−0.55 V vs. RHE, 75–100 mA cm^{-2}) (Fig. 8a) [118].

This layered structure in question offers three distinct advantages. Firstly, the presence of a polytetrafluoroethylene (PTFE) porous diffusion protection layer serves to slow down the diffusion rate of CO_2, allowing for its reduction to occur prior to any side reactions with the strongly alkaline electrolyte. Additionally, the rate of the competitive HER reaction is also slowed down in alkaline electrolytes, thereby further improving the selectivity of electrocatalytic reduction to C_2H_4. Secondly, as a significant amount of CO_2 is reduced prior to encountering OH^-, a large quantity of OH^-

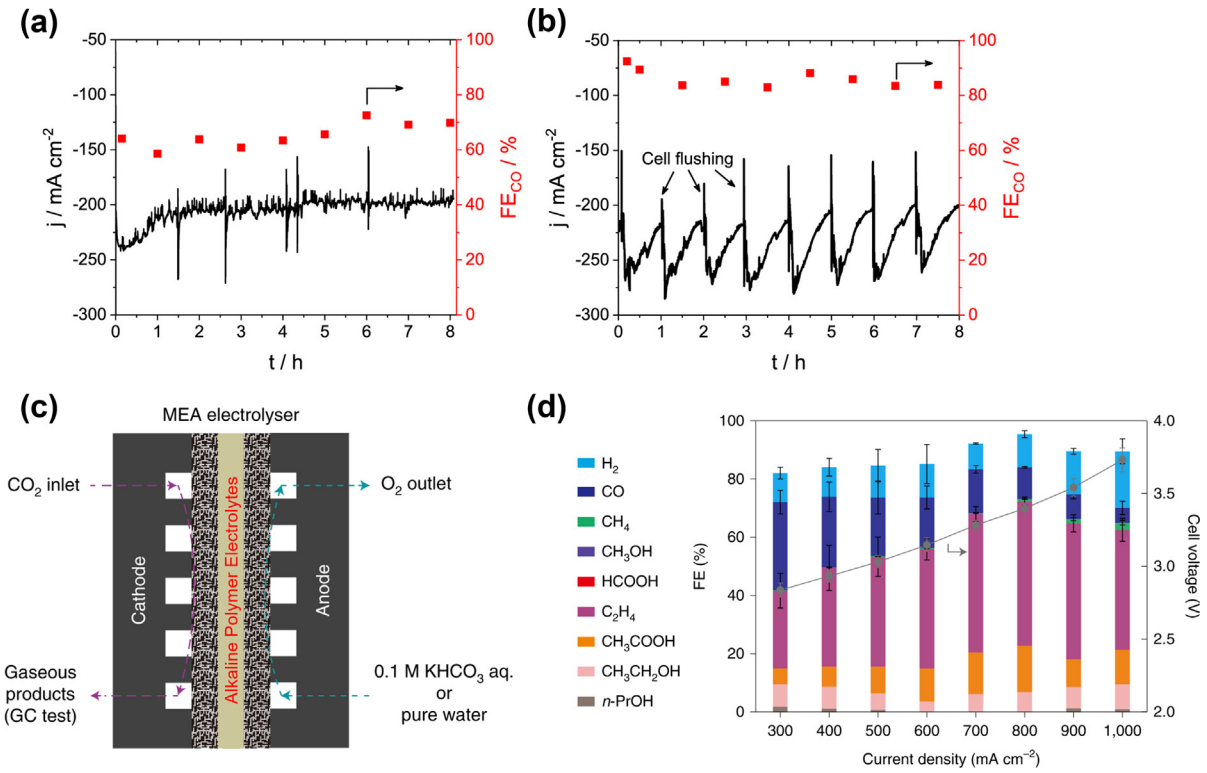

Fig. 7. Chronoamperometric curves recorded at $\Delta U = -3.00$ V with CO_2 flow rate = 750 cm^3 min^{-1}, humidified at (a) T = 85 °C and (b) T= 60 °C, while the cell was rinsed with ca. 50 cm^3 deionized water at the beginning of each hour. Reproduced with permission from [134]. Copyright 2019 American Chemical Society. (c) Structural illustration of the MEA electrolyzer with CO_2 and pure water co-electrolysis and (d) corresponding FEs toward various CO_2 reduction products. Reproduced with permission from Copyright 2022 Springer Nature.

can be adsorbed on the surface of the Cu metal catalyst. This, in turn, lowers the activation energy barrier for C–C coupling and enhances the selectivity of C_2H_4 even more. Lastly, the presence of the PTFE porous diffusion protection layer greatly enhances the stability of the Cu nanocatalyst, allowing it to function reliably for 150 h under working conditions. To further demonstrate the efficacy of their findings, the research team constructed an electrocatalytic reduction full cell system, consisting of a graphite/carbon NPs/Cu/PTFE cathode electrode and a $NiFeO_x$ anode electrode, which archives EE of 34% [118,124].

Additionally, the electrocatalytic system composed of carbon paper/PTFE coated carbon/Cu-KOH electrode, created by mechanically blending Cu nanoparticles with KOH solids, demonstrates remarkable performance in the CO_2RR-to-C_2H_4 process. This system incorporates an interactive flow channel between the anode and cathode, promoting the efficient flow of the electrolyte liquid to mitigate cathodic overpotential and ion transport resistance. In the zero-gap GDE design, the Cu-KOH catalyst, integrated with KOH, achieves a high current density of 281 mA cm^{-2} and a high selectivity for C_2H_4 with FE of 54.5% (Fig. 8b) [171]. Previous research has primarily focused on functional Cu-based composites in the catalyst layer of GDE, neglecting the presence of non-reactive polymers such as ionomers. However, recent studies have demonstrated that non-metric interactions at the catalyst-ionomer interface can significantly impact the local microenvironment on the cathode. By introducing an anti-swelling anion-exchange ionomer (AEI) with -$N(CH_3)^{3+}$ groups and an anti-swelling backbone, carbon fibre/microporous layer/AEI-OD-Cu nanosheets were synthesized (Fig. 8c). This novel strategy of enhancing the non-reactive ionomer in the catalyst allowed the gas-fed catalyst system to achieve a remarkable 60% selectivity for C_2H_4, coupled with an extremely high current density of 800 mA cm^{-2} [143,172].

4. Innovative perspectives on CO_2RR-to-C_2H_4 process

4.1. Machine learning in electrocatalyst screening

Machine learning (ML) is currently experiencing a resurgence, that is having a significant impact on various science and engineering fields, including CO_2RR. ML entails the construction of models using data, allowing for the discovery of hidden relationships within vast amounts of data [173–178]. ML takes a unique approach to model development, relying on flexible and non-linear models. This characteristic enables ML to identify intricate non-linear relationships within datasets and predict the CO_2RR activity of unknown electrocatalysts [176]. Additionally, ML does not require extensive prior knowledge of output features, making it possible to obtain a trained model based on reference data and generate the required information [179]. ML-assisted functional material design and screening strategies can greatly reduce time and resource costs in the research journey from lab to fab for CO_2-RR-to-C_2H_4 [180,181]. A general ML-assisted electrocatalytic CO_2 reduction workflow consists of four main steps: setting up the data source/data feed, selecting and validating the descriptors, defining the algorithm, and validating the model and making predictions (Fig. 9 and 10a–d) [178,182,183].

The identification of cathode materials for CO_2 conversion involves analyzing several features, including the d-band centre, adsorption energy, and number of ligands present in the electrocatalyst material. These features are essential in predicting the performance of CO_2RR. Calculations and statistical analysis of these descriptors enable the evaluation of unknown catalyst components, active sites, and the exploration of CO_2RR pathways. Consequently, these features serve as crucial descriptors in ML tasks.

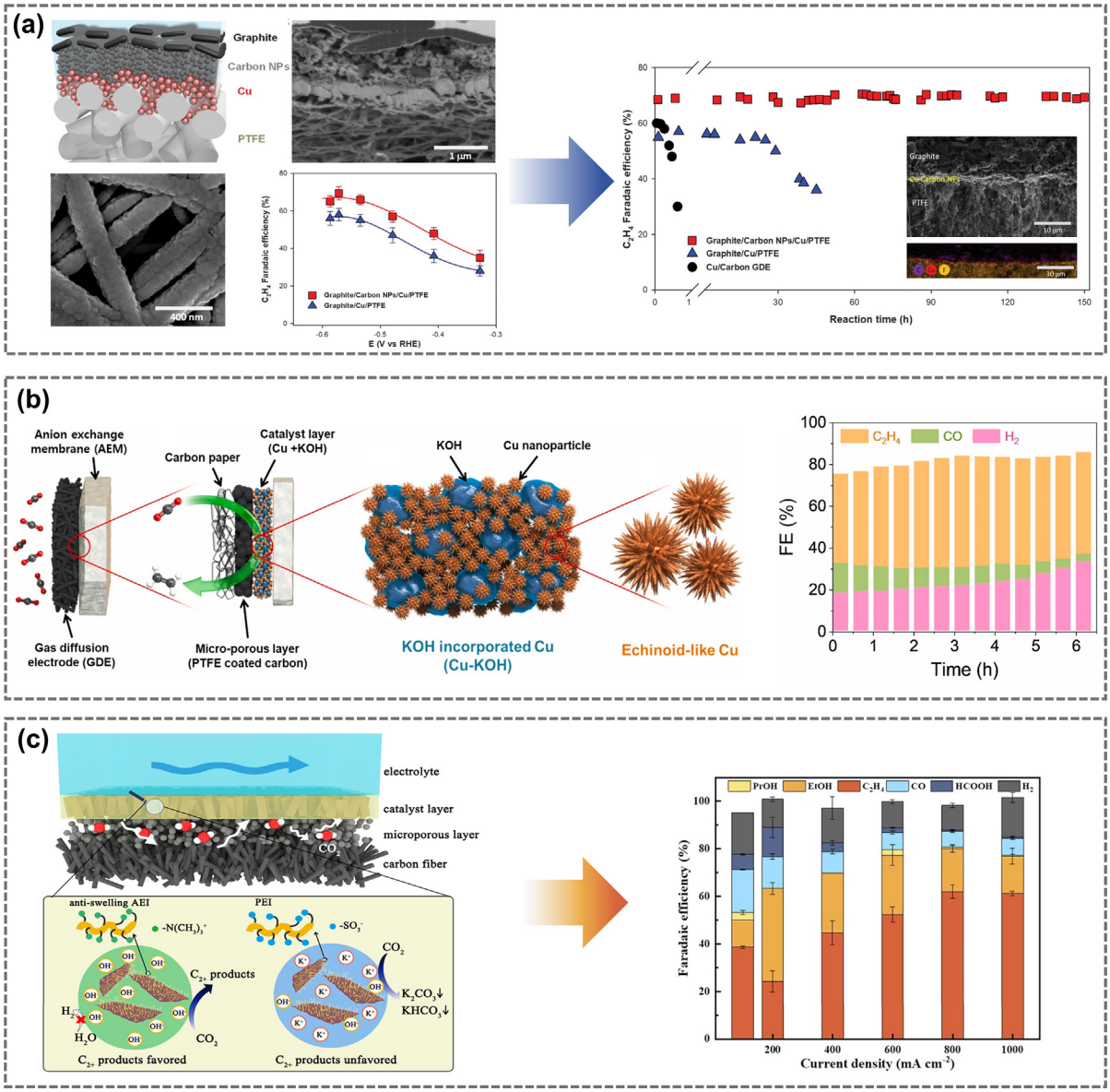

Fig. 8. (a) Structure, FE_{C2H4}, and 150-h stability test of the graphite/carbon NPs/Cu/PTFE electrode. Reproduced with permission from [118]. Copyright 2018 American Association for the Advancement of Science. (b) Schematic illustrations of KOH-incorporated Cu (Cu-KOH) electrodes; FEs of C_2H_4, CO and H_2 by Cu-KOH electrode. Reproduced with permission from [171]. Copyright 2021 Elsevier. (c) Manipulation of CO_2-to-C_{2+} activity and selectivity through local environment construction; FEs for C_{2+} products over the AEI-OD-Cu nanosheets. Reproduced with permission from [172]. Copyright 2022 American Chemical Society.

However, these descriptors require time-consuming Density Functional Theory (DFT) calculations, especially when dealing with a vast range of potential catalyst materials [184–186]. To overcome computational limitations associated with DFT calculations, ML can extract rules from a sufficient amount of DFT-computed data and apply these rules to efficiently predict target properties [173,187]. This ML-assisted approach is particularly effective in the field of electrocatalytic CO_2 reduction, especially in high-throughput multi-scale materials screening and catalysts design [183,188]. For example, the combination of ML and DFT calculations demonstrates significant advantages in assessing the catalytic activity of transition metal phthalocyanine (TMPc) dual-metal-sites catalysts (DMSCs) for CO_2RR (Fig. 10e). It is reported that the combined ML-DFT strategy is 130,000 times faster than using DFT calculations alone when screening and evaluating single-atom catalysts [189]. These findings highlight the superior performance of the ML-DFT approach in predicting the reactivity of electrocatalysts in CO_2RR, such as single atom catalysts [190], high entropy alloy catalysts [191] and metal-zeolites catalysts [192].

The hybrid scheme of DFT-ML exhibits a remarkable low prediction error of 0.02 V, along with a substantial nearly seven-fold enhancement in efficiency [193]. Additionally, the proposition of ML models incorporating active learning is an intriguing avenue. An example of this approach involves employing an ML model based on active screening to guide high throughput calculations in DFT, specifically in the screening of CO_2RR catalysts with exceptional performance in a materials library by predicting the adsorption energy of CO (Fig. 10a–d) [187]. For CO_2RR-to-C_2H_4, theoretical findings indicate that the Cu-Al alloy exhibits the highest activity and selectivity, particularly with regards to the Cu-Al catalyst displaying relatively higher FE of C_2H_4 [182]. Apart from substrate catalyst prediction and screening, ML has played a guiding role in the discovery and optimization of organic molecular

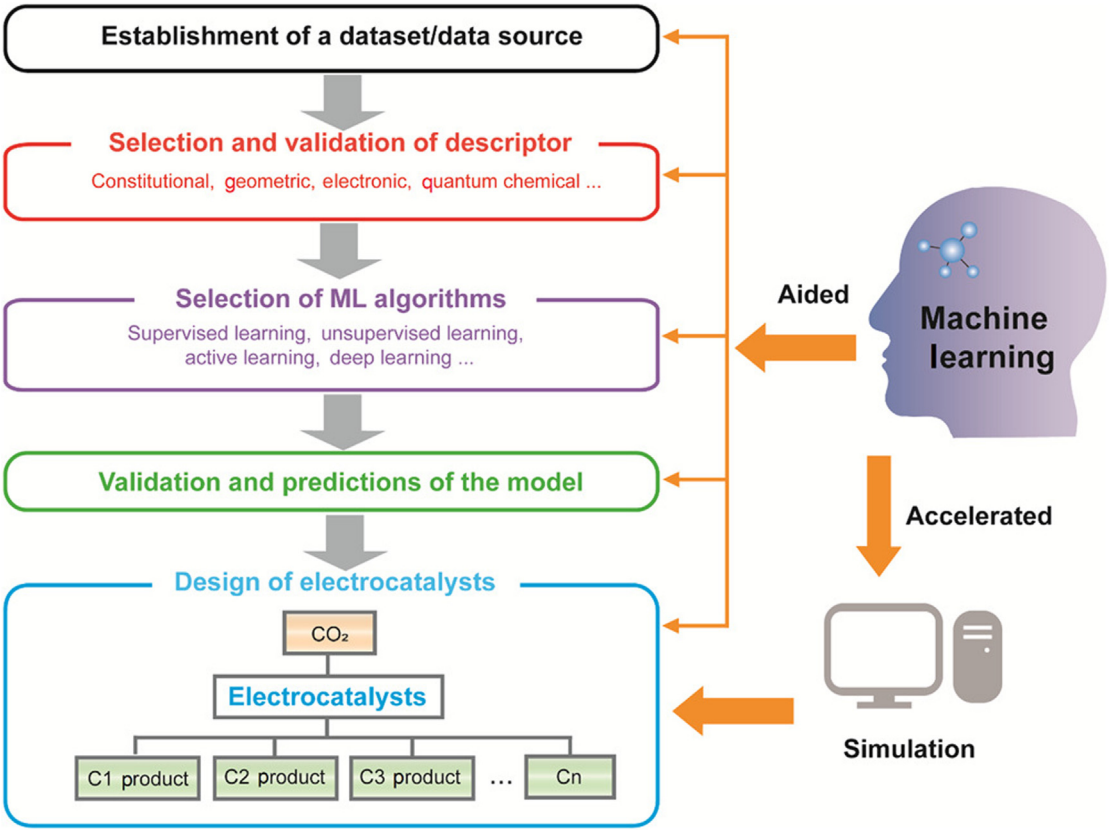

Fig. 9. Schematic illustration of ML-accelerated computation and design of electrocatalysts for CO_2 reduction reaction. Reproduced with permission from [183]. Copyright 2022 John Wiley and Sons, Inc.

additives in Cu-based electrode electrodeposition, leading to achievement of high selectivity for CO_2RR-to-C_2H_4. The data analysis process in this research involved three iterative cycles: identification of significant features, refinement of critical features, and catalyst design and validation. Through this work, a combination of aliphatic alcohols and Cu_2O was determined and selected from a pool of over 2000 potential formulations consisting of 200 organic additives and 12 metal salts. Experimental results further confirmed the aliphatic alcohol promoted Cu_2O cubes' high selectivity (>50%) for C_{2+} products (Fig. 10f) [194].

4.2. Value-added co-electrolysis

4.2.1. Mixed-feed electrolysis

The development and mechanistic studies of catalysts have predominantly utilized traditional pure CO_2 feeds [195]. However, the incomplete combustion of carbon-based fuels often results in a mixture of CO and CO_2 gases. This emphasizes the scientific significance and potential application of electrocatalytic reduction of CO/CO_2 gas mixtures [196]. Additionally, impure, or frequently contaminated CO_2 feeds are common in industrial settings, necessitating a more in-depth mechanistic study of CO_2RR-to-C_2H_4 under O_2/CO_2 and CO/CO_2 co-feed conditions [196,197]. Recent experiments have shed light on the relationship between Cu catalyst surface species and catalytic performance by introducing an oxidant (oxygen) into the CO_2 feed [198]. The introduction of oxygen into the reactor facilitates the oxygen reduction reaction (ORR). By adopting a co-feeding strategy, the fractional current density of the desired C_2H_4 at a potential of −0.75 V vs. RHE increases 173-fold and there is a 200 mV shift in the onset potential of CH_4 production towards the equilibrium potential (Fig. 11a) [198]. In addition to incorporating oxidizing media into the CO_2 feed, the electrocatalytic reduction of CO/CO_2 gas mixture holds significant practical importance. Dynamic isotope labelling-based experiments have revealed that the mixed CO/CO_2 feed considerably enhances the rate of C_2H_4 production (Fig. 11b). Moreover, the presence of non-competitive surface sites for CO/CO_2 adsorption on the catalysts has been identified through the examining of reaction surfaces containing reaction-specific sites [196].

4.2.2. CORR and GOR

In addition to CO/CO_2 co-feeds, the production of C_2H_4 through direct electrochemical CO reduction reaction (CORR) is being explored as a viable approach to ensure a sustainable carbon cycle. High FE of 52.7% was achieved by optimizing the cathode structure to enhance CO diffusion and C–C coupling at the electrode surface (Fig. 11c) [197]. Importantly, this highly selective process for producing C_2H_4 results in minimal production of other carbon-based by-products, such as C_1—C_4 hydrocarbons and CO_2, thereby avoiding the drawbacks associated with uneven product distribution in conventional pure CO_2 feed processes. Furthermore, Sinton and Ramdin et al. have investigated the concept of heterogeneous co-electrolysis, which involves the simultaneous direct reduction of CO on the cathode and glycerol oxidation (GOR) on the anode [195,199]. This strategy of hybridizing the cathode and anode not only reduces the energy input for C_2 cathode products but also generates valuable C_3 products with a significant market demand on the anode. The experimental results demonstrate that a high rate of co-production of valuable C_2 and C_3 product streams can be achieved at a full cell potential of 1.34 V, with a current density of 180 mA cm^{-2}. Besides, the cathode primarily yields ethylene (C_{2+}: FE = 71%, C_2H_4: FE > 45%), while the anode produces lactic

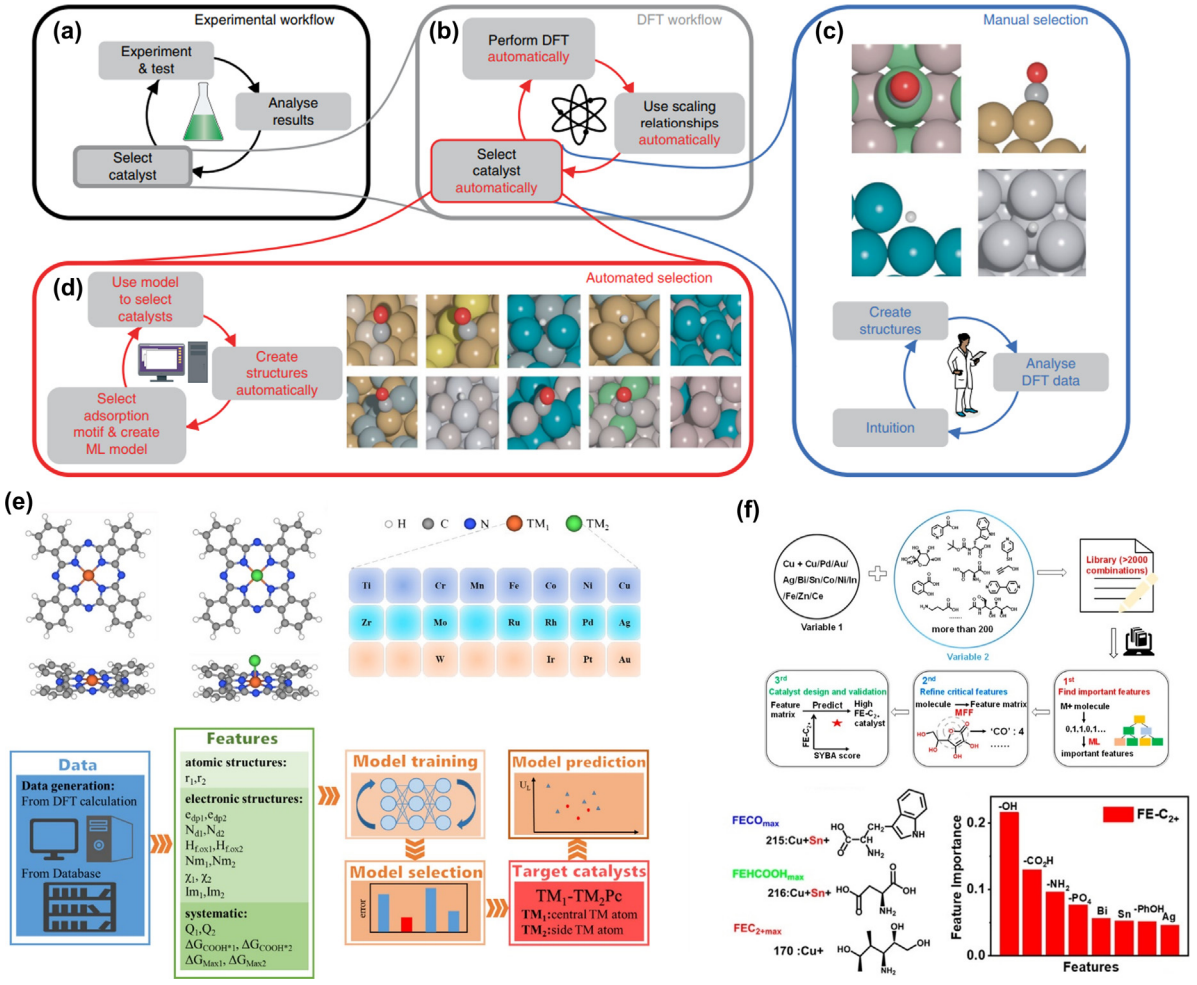

Fig. 10. (a–d) Schematic illustration of workflow for active learning of intermetallic compounds to guide the discovery of CO_2 reduction electrocatalysts. Reproduced with permission from [182,187]. Copyright 2020 & 2018 Springer Nature. (e) Structures of TMPc and TM_1-TM_2Pc, respectively. All screened transition metal elements and schematic diagrams of the inner procedure of the ML-accelerated catalytic activity prediction of Pc DMSCs. Reproduced with permission from [193]. Copyright 2021 American Chemical Society. (f) The learning loop for accelerated discovery based on three iterative cycles of "experimental test–ML analysis–prediction and redesign" to guide the search for high-performance CO_2RR catalysts. FE_{C2+} obtained by gradient boost decision tree regression analysis for the first round ML. Reproduced with permission from [194]. Copyright 2021 American Chemical Society.

acid and glyceric acid (C_{3+}: FE = 75%) (Fig. 11d). By integrating the system, the projected energy cost of producing C_2H_4 from CO_2 can be reduced by 50%, as the energy requirement for the conversion of CO to C_2H_4 is decreased by 55% (to approximately 72 GJ ton^{-1} C_2H_4) [199].

4.3. Cascade processes

As previously discussed, the tandem catalyst system divides the CO_2-to-C_2H_4 pathway into a pre-stage of CO_2-to-CO and a post-stage of CO-to-C_2H_4. Nevertheless, this particular micro-scale design of the material structure cannot completely prevent the loss of reaction materials, such as carbonate precipitation and the challenges associated with low CO_2 conversion rates [200]. Therefore, a CO_2-to-C_2H_4 cascade process is of practical significance in addition to the direct conversion route. Ozden et al. have developed a cascade method for converting CO_2 to C_2H_4 by integrating a solid oxide electrochemical cell (SOEC) of CO_2-to-CO with a high-performance MEA system for CO-to-C_2H_4. This approach effectively avoids carbonate formation and the resulting energy losses, leading to excellent overall performance and enhanced feedstock utilization. In their study, the researchers initially designed a layered catalyst consisting of Cu, $(C_4HF_7O_4S.C_2F_4)_x$, a short-side-chain (SSC) ionomer, and N-tolyl substituted tetrahydrobipyridine in an MEA electrolyzer, which achieves efficient conversion of CO to C_2H_4. Furthermore, to prevent CO_2 loss in the alkaline electrolyte during CO_2 conversion, an SOEC was connected to the front section of the MEA electrolyzer to enable high-rate conversion of CO_2 to CO. The MEA reactor demonstrates the ability to generate C_2H_4 at a maximum rate of 1.3 mmol h^{-1} and operates continuously for 40 h, benefiting from the efficient CO output from the SOEC (Fig. 12a) [142]. In addition to the SOEC-MEA process, a recent proposal has introduced a cascade strategy encompassing both electrocatalysis and thermal catalysis. More specifically, the outlet of the MEA electrolytic cell is directly linked to the inlet of a thermochemical hydroformylation reactor. Although the final products of this electrochemo-thermochemical reaction process, mainly ethane and C_3 oxygenates, this notable attempt showcases the potential of a cascade process that produces desired C_2H_4 at a high conversion rate and yield (Fig. 12b) [201]. Consequently, there exists a prospect for future innovation and optimization of series processes by maximizing feedstock utilization and catalytic reforming.

4.4. Cell stacking

While MEAs represent a favorable option among various types of electrolyzers, it is important to acknowledge that the conventional MEAs used in laboratory settings are not suitable

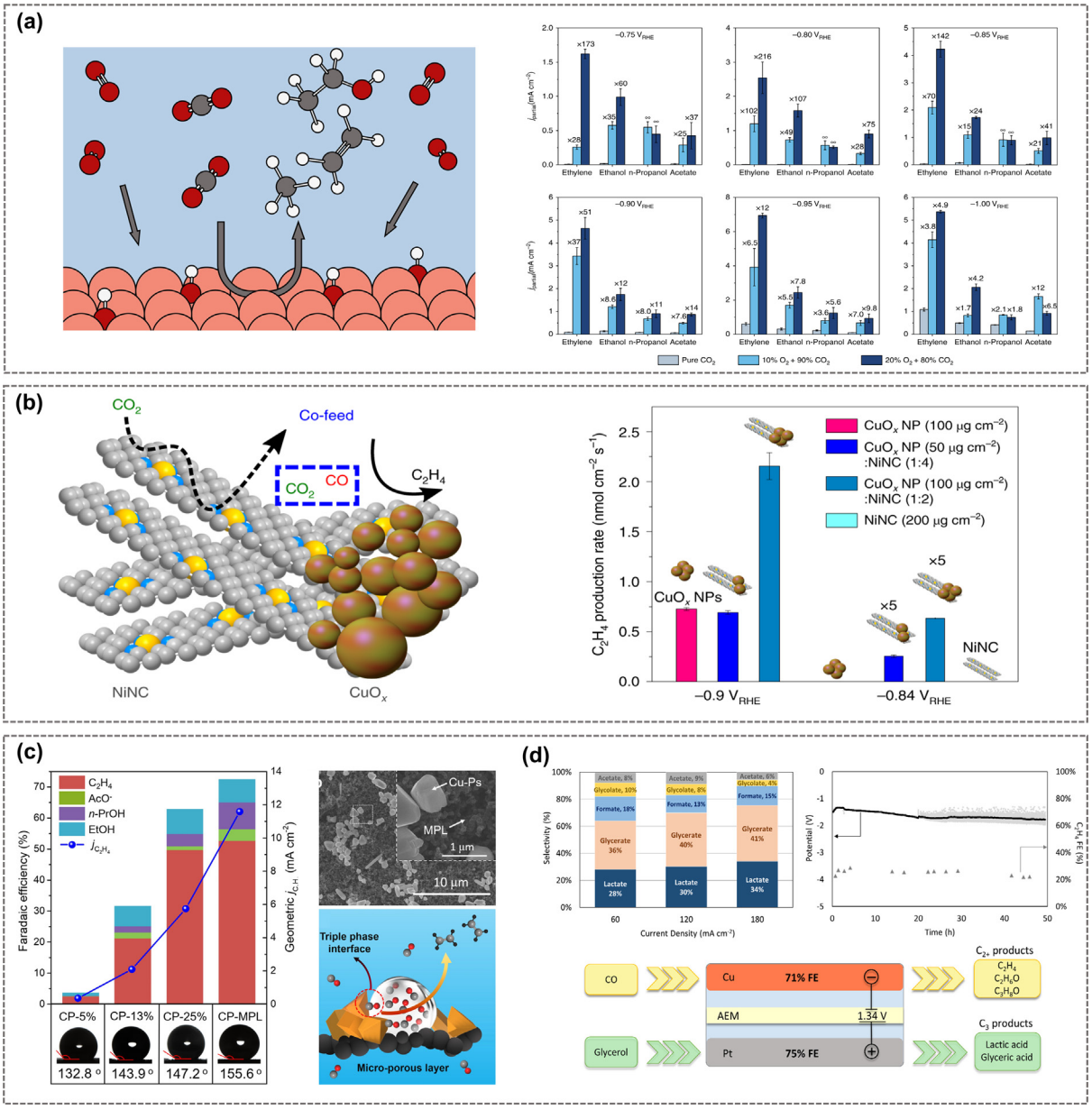

Fig. 11. (a) Schematic diagram of oxygen-induced promotion of CO_2RR. The partial current densities of C_{2+} products are compared at various potentials, specifically at 100% CO_2, 10% O_2 + 90% CO_2, and 20% O_2 + 80% CO_2. These numbers represent the enhancement relative to the rates observed with pure CO_2. Reproduced with permission from [198]. Copyright 2020 Springer Nature. (b) The tandem catalyst design combines Ni-N-doped carbon matrix (as a local CO producer) and CuO_x NPs on GDE. C_2H_4 formation rate with different bifunctional hybrid catalysts. grey: C atoms; blue: N atoms; yellow: Ni atoms. Reproduced with permission from [196]. Copyright 2019 Springer Nature. (c) Schematic illustration for electrocatalytic CO reduction process on Cu catalysts with the assistance of the hydrophobic micro-porous layer to improve the CO diffusion. Reproduced with permission from [197]. Copyright 2020 John Wiley and Sons, Inc. (d) Diagram of the electrochemical CO reaction combining the oxidation of glycerol for cathode and anode within MEA reactor. Selectivity at different current densities and a 50-h stability test. Reproduced with permission from [199]. Copyright 2021 American Chemical Society.

for large-scale production of C_2H_4. To achieve this goal, scaled and modified MEA need to be explored, such as the construction of larger electrolytic cells or the interconnection of multiple electrolytic cells [136,171,202]. Fig. 13 illustrates these strategies and their potential for enabling the commercialization of C_2H_4 production through electrolysis. There are two configurations for cell stacking in a stack assembly: parallel connection and series connection. In the parallel configuration, the cells are interconnected in a way that ensures uniform gas distribution across the layers, where each cathode receives a dedicated supply of CO_2 (Fig. 13a). On the other hand, in the series configuration, the entire gas flux enters the first layer, while the off-gas, consisting of residual CO_2 and reaction products, proceeds to subsequent layers (Fig. 13b) [134]. From an electrical perspective, the cells are connected in series in both scenarios. Compared to the large-scale electrolytic cells, the construction and maintenance of the stack is more convenient, and the single-layer electrolytic cell in the stack is similar to the one in laboratory setting. In terms of electrochemical devices, series stacks have shown higher conversion efficiencies compared to stacks with electrolytic cells in parallel. Results have supported the idea that

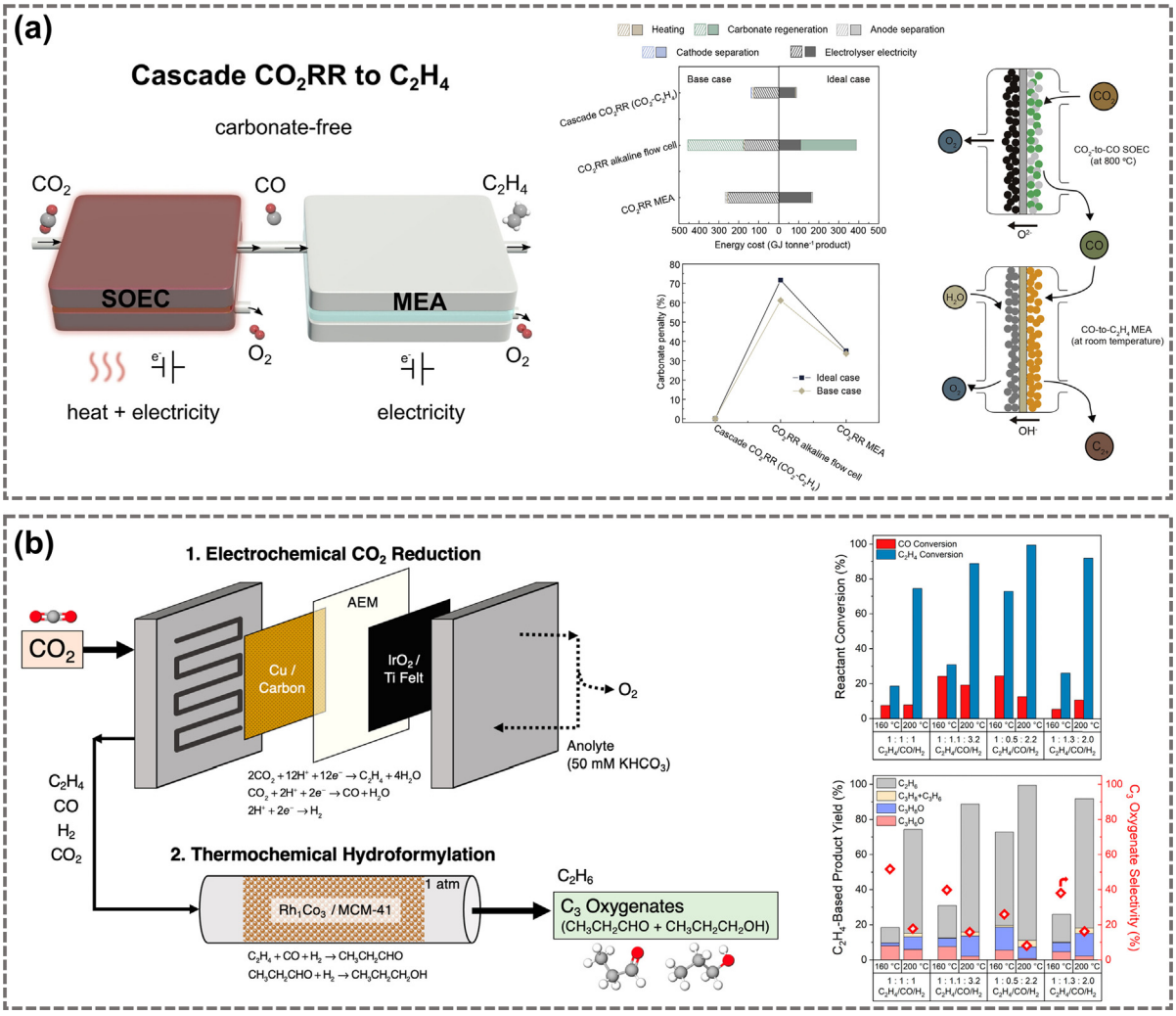

Fig. 12. (a) Schematic illustration of the SOEC-MEA cascade approach for carbonate-formation-free CO_2-to-C_2H_4 conversion. Comparison of energy cost and carbonate penalty for three electrolysis systems. Reproduced with permission from [31,142]. Copyright 2021 Elsevier & American Chemical Society. (b) Schematic illustration of tandem electrochemical-thermochemical reactors toward CO_2 conversion to C_3 oxygenate products. Reactant conversion and C_2H_4-based product yield of different gas feeding. Reproduced with permission from [201]. Copyright 2022 American Chemical Society.

stacks with a series configuration can enhance CO_2 conversion within a stack, thereby achieving a remarkable current density of 300 mA cm^{-2} [134,203].

5. Techno-economic analysis of CO_2RR-to-C_2H_4 process

The market price of each CO_2RR product is detailed in Table S5. At present, carbon monoxide and formic acid are economically viable products with significant net present value (NPV) of $13.5 million and $39.4 million, respectively, for the CO_2 electrolyzer system [204–206]. Additionally, C_2H_4, a chemical precursor, fuel additive, and energy generation fuel, is commonly utilized as a feedstock for the production of polyethylene, ethylene oxide, and ethylene glycol, among other feedstocks [207]. The annual global production of C_2H_4 stands at 150 million metric tons with a favorable price point of 1.3 USD per kilogram, highlighting its considerable economic significance [132].

5.1. CO_2 capture, product separation and storage

In a typical CO_2RR process, as depicted in Fig. 14(a), CO_2 is extracted from a point source or air and is subsequently purified for utilization in a CO_2 electrolysis system [132]. Currently, the prevailing technique for CO_2 capture is chemisorption using monoethanolamine, a method that incurs substantial operational costs totalling $70 per ton of CO_2 captured [208]. Previous research efforts have shown that the expenses associated with CO_2 capture can be reduced to $44 per ton through improvements in solvent composition and process optimization [136]. In addition, the generation of value-added products from CO_2RR can contribute to the economic viability of CO_2 capture. It is worth noting that the CO_2 captured from point sources may contain other combustion products (such as SO_x and NO_x), that could potentially impair the electrolyzer performance [132,209]. To ensure stable and efficient conversion, the CO_2 may require high purity [210]. On the other hand, in contrast to CO_2 capture from point sources of industrial facilities, direct extraction of CO_2 from the atmosphere allows for decentralized utilization and can be effectively integrated with renewable energy sources. However, it is important to highlight that this particular facility has yet to be commercially developed [211].

Following the raw capture of CO_2, the concentrated CO_2 mixture is combined with water and then transferred to CO_2 electrolytic cells. The resulting liquid product within the electrolyte stream is then sent to a separation system, specifically distillation, in order

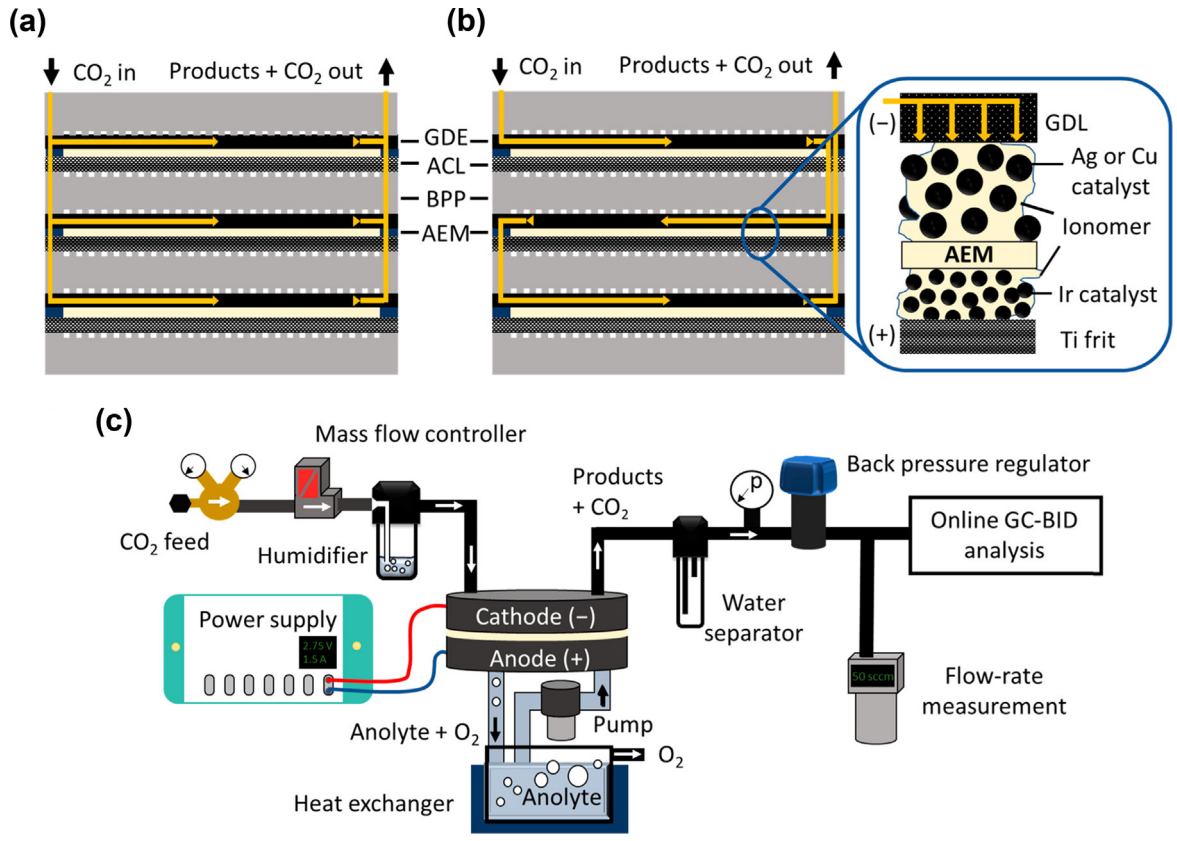

Fig. 13. The structure of the CO_2 gas channel in an electrolyzer stack, comprising three layers, can be illustrated in (a) parallel and (b) serial connection configurations. The components involved include the bipolar plate (BPP), anode catalyst layer (ACL), gas diffusion electrode (GDE), gas diffusion layer (GDL), and anion exchange membrane (AEM). Furthermore, (c) a schematic flowchart of the measurement setup provides an overview of the experimental arrangement. Reproduced with permission from [134]. Copyright 2019 American Chemical Society.

to extract the liquid product. At the same time, the electrolyte is recycled back to the electrolysis device [132,212]. The gaseous product, consisting of the unconverted feed gas (CO_2) and the by-product (H_2), undergoes separation within a gas separation unit. Within this unit, the recycled CO_2 is returned to the reactor, while the gas product is subsequently compressed for storage and transportation purposes. Alternatively, it can be directed towards another subsequent chemical process [213,214]. Pressure swing adsorption (PSA) is a widely employed industrial technique utilized for the separation of gaseous products. It is renowned for its advantageous attributes, including low operating costs, high efficiency, and a compact footprint. PSA is considered as a reference process within the industry, with a cost estimate of \$1,990,000 per 1000 m^3 per hour [215–217]. Subsequently, it is necessary to compress and store the gaseous products after the separation process. However, if these products are promptly transported to a subsequent process and utilized without delay, the associated additional cost can be deemed insignificant. Jiao's analysis, presented in Table S6, offers an overview of the estimated costs in a generalized CO_2RR process. Notably, the analysis takes an optimistic perspective, anticipating potential cost reductions resulting from future technological advancements [132].

5.2. Electricity and CO_2 costs

Based on extensive contemporary reports and the prevailing operational conditions, it has been observed that among the products obtained through CO_2RR, CO and formic acid demonstrate profitability, while the production of C_2H_4 appears to lack economic viability [21,218–221]. Notably, with the continuous advancements in CO_2RR technology, it is worth mentioning that C_2H_4 emerges as a financially sustainable product when technological enhancements are implemented [117,222]. A production rate of 100 t d^{-1} allows for large-scale chemical production with more favorable capital costs, and further electricity prices may decrease to 0.03 USD kWh^{-1} as renewable energy sources such as solar and wind become more affordable [132,153]. Experimental findings indicate that CO_2 conversion during CO_2RR can reach nearly 35% and may surpass 50% with an improved electrolyzer design [223,224]. An analysis of a reactor with a 50% conversion rate yields an NPV of \$24 million for C_2H_4 when FE is calculated at 90%, the cell voltage is 2 V, and the current density is 300 mA cm^{-2} [132].

Throughout the entire duration of ethylene production, the cost of production process assumes paramount significance. Fig. 14(b), which illustrates the breakdown of production costs, highlights the substantial portion is attributed to electricity cost [132]. It is projected that as the new energy industry continues to advance, the integration of various power generation technologies such as wind power, hydropower, nuclear power, and solar power will contribute to a decline in electricity prices [215]. In fact, it is anticipated that the cost of electricity can potentially be reduced to as low as 0.02 \$ kWh^{-1} [225]. A mere alteration of \$0.01 kWh^{-1} in the electricity tariff would result in a substantial divergence in the NPV, amounting to nearly \$40 million [132]. This modification would have a significant impact on the production of C_2H_4, especially when compared to the current price of 0.05 \$ kWh^{-1}. Consequently, it is crucial for CO_2 electrolyzers to ensure a reliable and affordable supply of electricity, preferably through the advancement of alternative energy sources such as wind power and solar power [215]. In addition to the

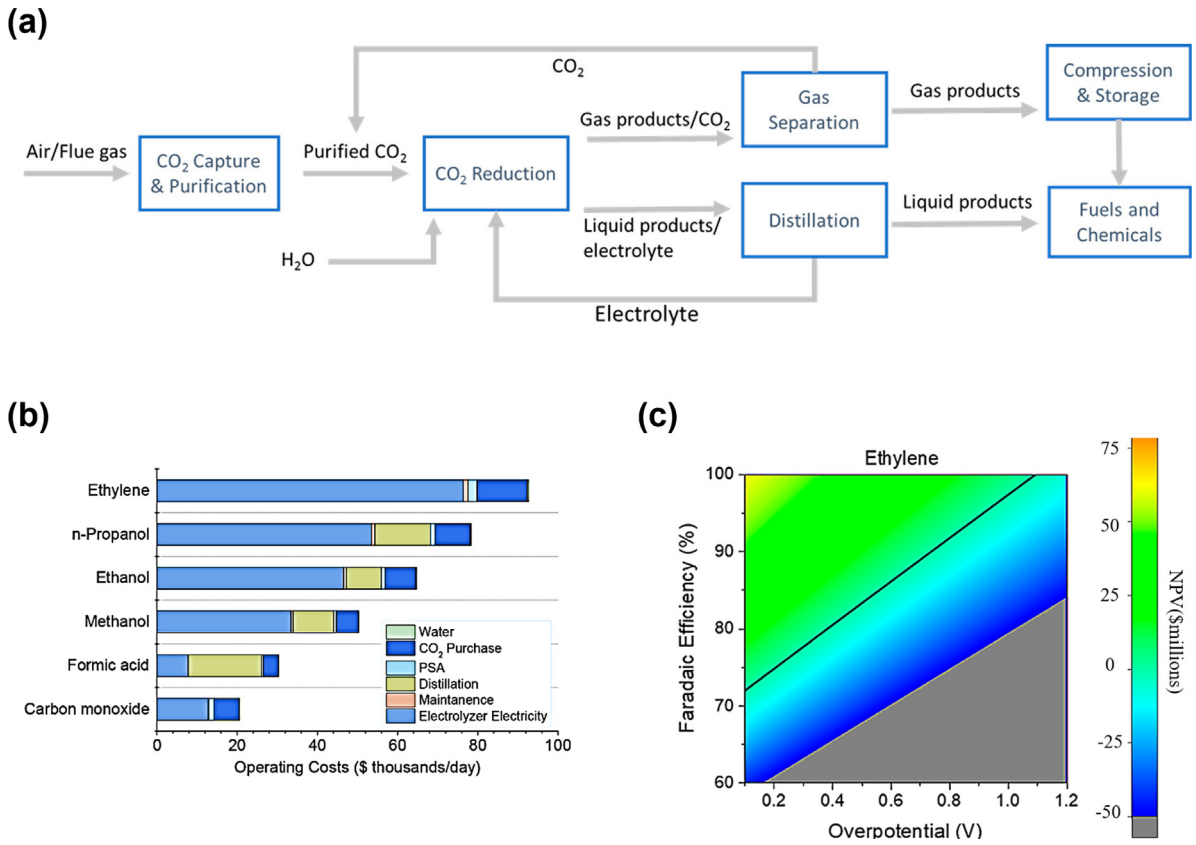

Fig 14. (a) General CO_2RR process flow diagram. (b) Operating costs for various products and (c) Dependence of end-of-life NPV on overpotential and selectivity with a current density of 300 mA cm^{-2}, solid line depicts an NPV of $0. Reproduced with permission from [132]. Copyright 2018 American Chemical Society.

expense associated with power, as solvent and process design improvements, the price of CO_2 could potentially decrease from $70 to $44 per ton [132,226]. Moreover, if carbon neutrality is adopted on a larger scale and industrialized, CO_2 prices may be further reduced. Considering all these factors, for the CO_2RR-to-C_2H_4 process to be profitable, the NPV must be greater than zero. As shown in Fig. 14(c), the solid line depicts the performance required to achieve $0 NPV for the production of C_2H_4 [132].

5.3. Loss cost: crossover and carbonate formation

As previously elucidated, the occurrence of crossovers within neutral MEA, the formation of carbonates in alkaline flow-cells, and the utilization of CO_2 below 100% in each respective system collectively result in significant CO_2 losses. These phenomena, which are inherent to the mentioned systems, lead to the dissipation of CO_2, thus reducing the overall energy efficiency associated with these technologies [31]. Specifically, as carbonate formation and crossover increase, the requirement for electrical energy efficiency rises so rapidly that it becomes unattainable. Tandem carbon dioxide reduction (TCO_2R), as a method for producing C_{2+} products, has been demonstrated to prevent the formation of carbonates from CO_2 [224,227–229]. Fig. 15(a) depicts the cost analysis of C_2H_4 production, considering varying ratios of crossover and carbonate formation in neutral MEAs and alkaline flow-cells. The observed slopes of the two distinct lines illustrate the significant impact exerted by crossover and carbonate formation on the overall cost of C_2H_4. Additionally, it is evident that the presence of crossovers and carbonate formation necessitates additional expenses for recovery processes, further increasing the overall production cost of C_2H_4.

Additionally, the cost breakdown of C_2H_4 production, as illustrated in Fig. 15(c), highlights the importance of considering the expenses related to CO_2 regeneration losses caused by carbonate formation in alkaline environments. This analysis offers valuable insights into the cost structure of C_2H_4 production in neutral MEAs and alkaline flow-cells, emphasizing the need to account for the costs incurred in CO_2 regeneration in alkaline settings. Based on laboratory data, these losses represent more than 60% of the total cost. Achieving ethylene production below $1000 t^{-1} without CO_2 losses would require an EE greater than 45%. As shown in Fig. 15, even with a low CO_2 crossover/carbonate formation ratio of 1:1, achieving $1000 t^{-1} C_2H_4 production would require an EE greater than 65%. The electrochemical conversion of CO_2 to CO with an EE of 80%, followed by alkaline electrolysis of CO with an EE of 40% for C_2H_4 production, has the potential to yield 1000 metric tons per annum of ethylene with an overall EE of 52% [31]. While this target is ambitious, it is deemed attainable within the context of the aforementioned electrochemical processes.

6. Conclusions and outlook

In summary, this article presents a systematic examination of the advancement made for the robust CO_2RR-to-C_2H_4 process from lab to fab. This review encompasses various aspects including the design strategies of Cu-based cathodic materials, the assembly of integrated electrolyzer devices, the innovative perspectives of CO_2-RR-to-C_2H_4 process, and an analysis of its economic viability using case studies. Nevertheless, there remain pressing challenges that necessitate immediate attention. To address these challenges, the following recommendations are put forth.

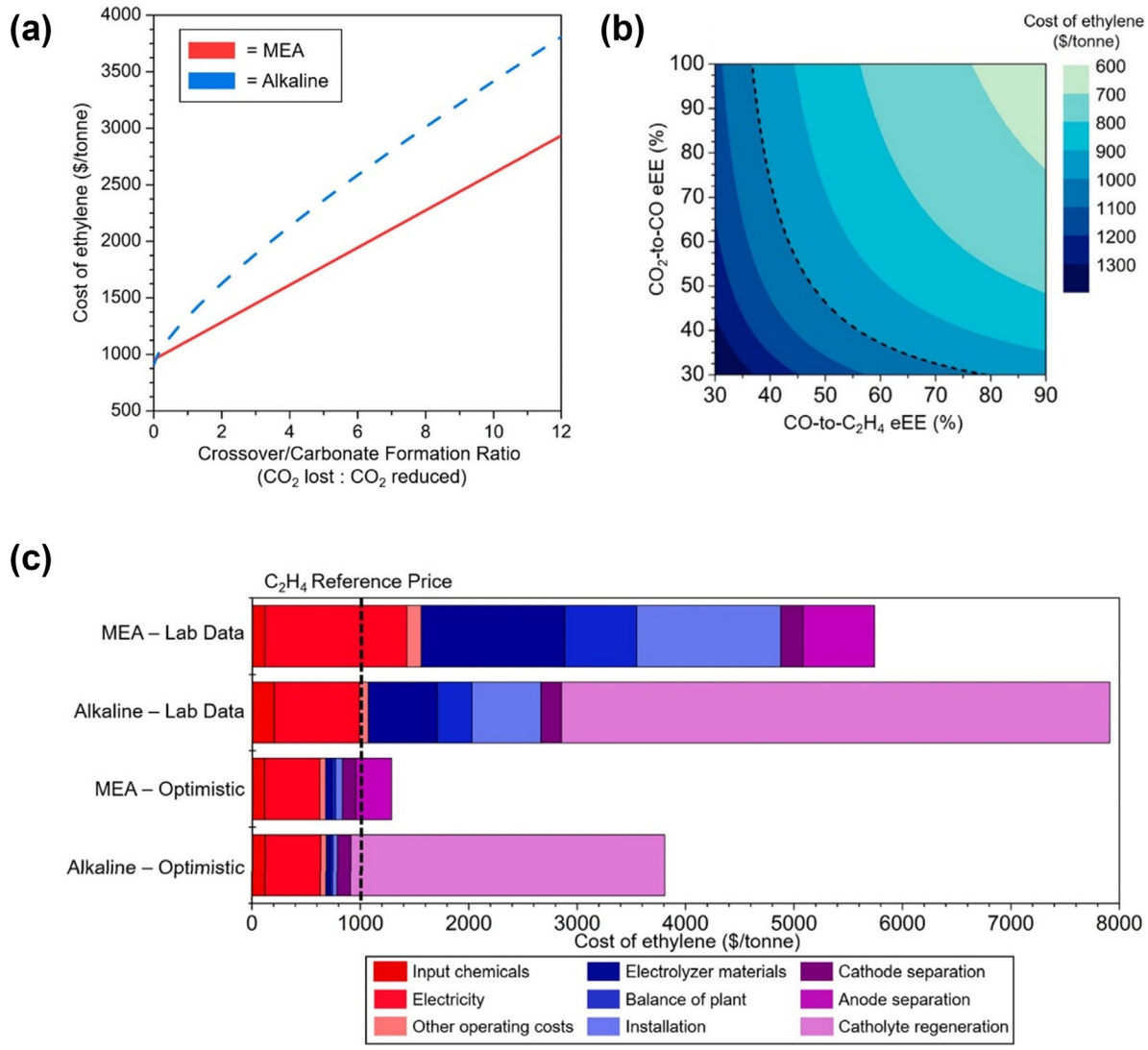

Fig. 15. (a) C_2H_4 production costs in neutral MEA and alkaline flow-cells with varying crossover/carbonate formation ratios. (b) Cost of ethylene with varying EE for each step of the reaction (CO_2-to-CO and CO-to-C_2H_4). The dotted black lines in all plots show ethylene's reference price (1000 \$ t^{-1}). (c) Cost of ethylene production breakdown for both CO_2RR and electrochemical CO reduction reaction (CORR) systems. Reproduced with permission from [31]. Copyright 2021 American Chemical Society.

1) **Structure-function relationships.** Numerous studies have been conducted on high-performance electrocatalysts for the conversion of CO_2 to C_2H_4. However, there remains a lack of comprehensive understanding of the structure–function relationships. For instance, the insights of the correlation between the adsorption strength of intermediates and the catalytic performance are pivotal for the rational design of catalysts. This lack of understanding directly impacts the reproducibility of related investigations in laboratory settings and the scalability in industrial applications. Additionally, the study of the dynamic evolution of cathode electrode material morphology, sectioning, and phases in multi-phase interfaces presents significant challenges. To overcome these obstacles, a combination of theoretical calculations and advanced spectroscopic techniques has proven to be advantageous. By utilizing in situ characterization techniques, even subtle changes at the material reaction interface during catalysis can be monitored, along with changes in relevant intermediates in CO_2RR. However, there is still an ongoing debate regarding the mechanisms of the CO_2RR-to-C_2H_4 process. Specifically, the C–C coupling pathway remains unclear. Insufficient evidence exists to determine whether the formation of the C_2 product results is solely a result of the coupling of two identical *CO intermediates or if it involves the simultaneous coupling of one *CO intermediate with other C_1 intermediates (such as *CHO or *COH). Moreover, it is still unclear whether the reaction pathways of CO_2-RR-to-C_2H_4 and CO_2RR-to-CH_4 are independent or if they compete.

2) **Electrolyzer.** The primary hurdle in implementing the findings of the fundamental research on CO_2RR-to-C_2H_4 at the industrial scale is the upscaling of the electrolyzer. Industrial electrolysis devices face various practical challenges, including the formation of (bi)carbonate after the reaction, deterioration of GDE performance, crossover issues, and catalyst poisoning. To achieve industrial-scale current densities, catalysis systems are using increasingly concentrated and corrosive electrolytes, which significantly impact the cost and lifespan of electrolyzer equipment. This deviation from the overarching goal of industrial conversion highlights the need to prioritize research to develop the optimal design for supporting infrastructure in industrial electrolyzer

installations, such as the use of neutral and acidic electrolytes. Additionally, there is significant interest in replacing highly concentrated solutions with less toxic, environmentally friendly, and recyclable electrolytes. These endeavours are crucial for advancing CO_2RR-to-C_2H_4 technology and bridging the gap between theoretical principles and practical applications.

3) **Scale-up.** In addition to electron selectivity and current density, it is crucial to consider parameters such as stability and single-pass conversion efficiency when evaluating the CO_2-RR-to-C_2H_4 systems. Regrettably, the investigation of stability has been largely overlooked in prior studies, and the operation time is mostly documented at low current densities, which holds limited importance for the industrialization of the CO_2RR-to-C_2H_4 process. To address the durability issue, it is imperative to investigate the dynamic changes over catalysts' surface during electrocatalytic reactions and the corresponding evolution of active sites. Subsequent research efforts have focused on developing mechanisms and solutions to cope with poisoning, carbon deposition, and degradation of catalyst materials. Additionally, it should be noted that increasing the CO_2 flow rate into the reactor at scale promotes the formation rate of the CO_2-RR product but reduces the proportion of CO_2 utilized, resulting in low single-pass conversion efficiency. Therefore, achieving a balance between the reaction rate and CO_2 utilization efficiency is crucial towards the scale-up of CO_2RR-to-C_2H_4 process.

4) **TEA.** The economic viability of the entire CO_2RR-to-C_2H_4 process is of paramount importance for its successful integration and commercialization. This encompasses several aspects, mainly including CO_2 capture, product separation and storage, electricity, and CO_2 cost. These areas are often overlooked in current laboratory research, so it is necessary to conduct a comprehensive techno-economic evaluation to determine the essential working parameters for the large-scale implementation of the CO_2RR-to-C_2H_4 process. However, one limitation of the discussed TEA is that it relies on extrapolating data from lab-scale experiments to predict the performance at fab-scale electrolyzer units, which may introduce uncertainties. Moreover, there is potential for further improvements in various domains of the TEA, which could enhance the economic and environmental benefits of the CO_2RR-to-C_2H_4 process. For instance, reducing electrolyzer costs can be achieved by minimizing material expenses, increasing current densities, and reducing overpotentials. These measures would result in less wasted heat and lower cooling costs. If these development strategies can be implemented successfully, the CO_2RR-to-C_2H_4 process has the potential to become a profitable option as a renewable energy process.

Declaration of competing interest

The authors declare that they have no known competing financial interests or personal relationships that could have appeared to influence the work reported in this paper.

Acknowledgments

This work is supported by Zhejiang Provincial Department of Science and Technology under its Provincial Key Laboratory Program (2020E10018). A.W. expresses gratitude for the financial support from Fundamental Research Funds for the Central Universities (2022LHJH01-03, 2022ZFJH04, 2022QZJH14) and Pioneer R&D Program of Zhejiang Province (2022C03040). H.B.W. acknowledges the financial aid from National Natural Science Foundation of China (22005266), Zhejiang Provincial Natural Science Foundation (LR21E020003) and Fundamental Research Funds for the Central Universities (2021FZZX001-09). J.D.H is supported by the Royal Academy of Engineering under the Chairs in Emerging Technologies scheme (CiET2021_17). Z.G. acknowledges the University of Nottingham Ningbo China for providing a full PhD scholarship.

Appendix A. Supplementary data

Supplementary data to this article can be found online at https://doi.org/10.1016/j.jechem.2023.11.019.

References

[1] R. Lindsey, L. Dahlman, Climate. Gov 16 (2020).
[2] R. Sani, T.K. Dey, M. Sarkar, P. Basu, S.M. Islam, Mater. Adv. 3 (2022) 5575–5597.
[3] N. Armaroli, V. Balzani, Chem. Asian J. 6 (2011) 768–784.
[4] N.S. Lewis, D.G. Nocera, Proc. Natl. Acad. Sci. U.S.A. 103 (2006) 15729–15735.
[5] Z. Liu, Z. Deng, S. Davis, P. Ciais, Nat. Rev. Earth Environ. 4 (2023) 205–206.
[6] K.C. Divya, J. Østergaard, Electr. Power Syst. Res. 79 (2009) 511–520.
[7] J.-Y. Fang, Q.-Z. Zheng, Y.-Y. Lou, K.-M. Zhao, S.-N. Hu, G. Li, O. Akdim, X.-Y. Huang, S.-G. Sun, Nat. Commun. 13 (2022) 7899.
[8] S. Zhang, J. Wu, M. Zheng, X. Jin, Z. Shen, Z. Li, Y. Wang, Q. Wang, X. Wang, H. Wei, J. Zhang, P. Wang, S. Zhang, L. Yu, L. Dong, Q. Zhu, H. Zhang, J. Lu, Nat. Commun. 14 (2023) 3634.
[9] Q. Gao, B. Yao, H.S. Pillai, W. Zang, X. Han, Y. Liu, S.-W. Yu, Z. Yan, B. Min, S. Zhang, H. Zhou, L. Ma, H. Xin, Q. He, H. Zhu, Nat. Synth 2 (2023) 624–634.
[10] Y.-Q. Yan, Y. Chen, Z. Wang, L.-H. Chen, H.-L. Tang, B.-L. Su, Nat. Commun. 14 (2023) 2106.
[11] S. Rarotra, A.K. Singh, T.K. Mandal, D. Bandyopadhyay, Sci. Rep. 13 (2023) 10298.
[12] P. Xiong, H.-B. Zhao, X.-T. Fan, L.-H. Jie, H. Long, P. Xu, Z.-J. Liu, Z.-J. Wu, J. Cheng, H.-C. Xu, Nat. Commun. 11 (2020) 2706.
[13] H.H. Khoo, I. Halim, A.D. Handoko, J. CO_2 Util. 41 (2020) 101229.
[14] S. Nitopi, E. Bertheussen, S.B. Scott, X. Liu, A.K. Engstfeld, S. Horch, B. Seger, I.E. L. Stephens, K. Chan, C. Hahn, J.K. Nørskov, T.F. Jaramillo, I. Chorkendorff, Chem. Rev. 119 (2019) 7610–7672.
[15] W. Wu, H. Hu, D. Ding, Cell Rep. Phys. Sci. 2 (2021) 100405.
[16] X. Duan, J. Xu, Z. Wei, J. Ma, S. Guo, S. Wang, H. Liu, S. Dou, Adv. Mater. 29 (2017) 1701784.
[17] J. Qiao, Y. Liu, F. Hong, J. Zhang, Chem. Soc. Rev. 43 (2014) 631–675.
[18] Y.-C. He, D.-D. Ma, S.-H. Zhou, M. Zhang, J.-J. Tian, Q.-L. Zhu, Small 18 (2022) 2105246.
[19] A. Hermawan, T. Amrillah, V.N. Alviani, J. Raharjo, Z.W. Seh, N. Tsuchiya, J. Environ. Manag. 334 (2023) 117477.
[20] Y. Yang, F. Li, Curr. Opin. Green Sustainable Chem. 27 (2021) 100419.
[21] L. Fan, C. Xia, P. Zhu, Y. Lu, H. Wang, Nat. Commun. 11 (2020) 3633.
[22] J. Wang, S. Kattel, C.J. Hawxhurst, J.H. Lee, B.M. Tackett, K. Chang, N. Rui, C.-J. Liu, J.G. Chen, Angew. Chem., Int. Ed. 58 (2019) 6271–6275.
[23] F. Li, A. Thevenon, A. Rosas-Hernández, Z. Wang, Y. Li, C.M. Gabardo, A. Ozden, C.T. Dinh, J. Li, Y. Wang, J.P. Edwards, Y. Xu, C. McCallum, L. Tao, Z.-Q. Liang, M. Luo, X. Wang, H. Li, C.P. O'Brien, C.-S. Tan, D.-H. Nam, R. Quintero-Bermudez, T.-T. Zhuang, Y.C. Li, Z. Han, R.D. Britt, D. Sinton, T. Agapie, J.C. Peters, E.H. Sargent, Nature 577 (2020) 509–513.
[24] Y. Hori, in: C.G. Vayenas, R.E. White, M.E. Gamboa-Aldeco (Eds.), Electrochemical CO_2 Reduction on Metal Electrodes, Mod. Aspects Electrochem. 2008, pp. 89–189.
[25] A.R. Woldu, Z. Huang, P. Zhao, L. Hu, D. Astruc, Coord. Chem. Rev. 454 (2022) 214340.
[26] P. Saha, S. Amanullah, A. Dey, Acc. Chem. Res. 55 (2022) 134–144.
[27] S. Banerjee, C.S. Gerke, V.S. Thoi, Acc. Chem. Res. 55 (2022) 504–515.
[28] S. Chu, Y. Cui, N. Liu, Nat. Mater. 16 (2017) 16–22.
[29] H. Zeng, X.-J. Xie, M. Xie, Y.-L. Huang, D. Luo, T. Wang, Y. Zhao, W. Lu, D. Li, J. Am. Chem. Soc. 141 (2019) 20390–20396.
[30] J. Liu, K. Zhou, S. Ullah, J. Miao, H. Wang, T. Thonhauser, J. Li, Small 19 (2023) 2304460.
[31] J. Sisler, S. Khan, A.H. Ip, M.W. Schreiber, S.A. Jaffer, E.R. Bobicki, C.-T. Dinh, E. H. Sargent, ACS Energy Lett. 6 (2021) 997–1002.
[32] C.M. Gabardo, C.P. O'Brien, J.P. Edwards, C. McCallum, Y. Xu, C.-T. Dinh, J. Li, E. H. Sargent, D. Sinton, Joule 3 (2019) 2777–2791.
[33] A. Paturska, M. Repele, G. Bazbauers, Energy Procedia 72 (2015) 71–78.
[34] W. Ma, S. Xie, T. Liu, Q. Fan, J. Ye, F. Sun, Z. Jiang, Q. Zhang, J. Cheng, Y. Wang, Nat. Catal. 3 (2020) 478–487.
[35] Y. Zang, P. Wei, H. Li, D. Gao, G. Wang, Electrochem. Energy Rev. 5 (2022) 29.
[36] W. Ye, X. Guo, T. Ma, Chem. Eng. J. 414 (2021) 128825.
[37] M. Gattrell, N. Gupta, A. Co, J. Electroanal. Chem. 594 (2006) 1–19.
[38] Y. Xue, Y. Guo, H. Cui, Z. Zhou, Small Methods 5 (2021) 2100736.
[39] L.D. Meinert, G.R. Robinson, N.T. Nassar, Resources 5 (2016) 14.

[40] N. Brewster, R.T. Economics, Outlook for commodity markets, Rio Tinto Inc. MF Global Seminar, 2009.
[41] H.U. Sverdrup, K.V. Ragnarsdottir, D. Koca, Resour., Conserv. Recycl. 87 (2014) 158–174.
[42] F. Dattila, R. García-Muelas, N. López, ACS Energy Lett. 5 (2020) 3176–3184.
[43] H. Liu, Q. Huang, W. An, Y. Wang, Y. Men, S. Liu, J. Energy Chem. 61 (2021) 507–516.
[44] M. He, W. An, Y. Wang, Y. Men, S. Liu, Small 17 (2021) 2104445.
[45] C.W. Li, M.W. Kanan, J. Am. Chem. Soc. 134 (2012) 7231–7234.
[46] Z.-Z. Wu, F.-Y. Gao, M.-R. Gao, Energy Environ. Sci. 14 (2021) 1121–1139.
[47] J. Kim, W. Choi, J.W. Park, C. Kim, M. Kim, H. Song, J. Am. Chem. Soc. 141 (2019) 6986–6994.
[48] N. Martić, C. Reller, C. Macauley, M. Löffler, B. Schmid, D. Reinisch, E. Volkova, A. Maltenberger, A. Rucki, K.J.J. Mayrhofer, G. Schmid, Adv. Energy Mater. 9 (2019) 1901228.
[49] D.-H. Nam, P. De Luna, A. Rosas-Hernández, A. Thevenon, F. Li, T. Agapie, J.C. Peters, O. Shekhah, M. Eddaoudi, E.H. Sargent, Nat. Mater. 19 (2020) 266–276.
[50] K. Wieszczycka, K. Staszak, M.J. Woźniak-Budych, J. Litowczenko, B.M. Maciejewska, S. Jurga, Coord. Chem. Rev. 436 (2021) 213846.
[51] D. Kim, S. Yu, F. Zheng, I. Roh, Y. Li, S. Louisia, Z. Qi, G.A. Somorjai, H. Frei, L.-W. Wang, P. Yang, Nat. Energy 5 (2020) 1032–1042.
[52] Y. Park, J. Yoo, B. Lim, W. Kwon, S.W. Rhee, J. Mater. Chem. A 4 (2016) 11582–11603.
[53] R. Mout, D.F. Moyano, S. Rana, V.M. Rotello, Chem. Soc. Rev. 41 (2012) 2539–2544.
[54] L. Xue, X. Wu, Y. Liu, B. Xu, X. Wang, S. Dai, P. Liu, H. Yang, Nano Res. 15 (2022) 1393–1398.
[55] J. Li, F. Li, C. Liu, F. Wei, J. Gong, W. Li, L. Xue, J. Yin, L. Xiao, G. Wang, J. Lu, L. Zhuang, ACS Energy Lett. 7 (2022) 4045–4051.
[56] C. Kim, T. Eom, M.S. Jee, H. Jung, H. Kim, B.K. Min, Y.J. Hwang, ACS Catal. 7 (2017) 779–785.
[57] Z. Wang, K. Sun, C. Liang, L. Wu, Z. Niu, J. Gao, ACS Appl. Energy Mater. 2 (2019) 192–195.
[58] C. Kim, H.S. Jeon, T. Eom, M.S. Jee, H. Kim, C.M. Friend, B.K. Min, Y.J. Hwang, J. Am. Chem. Soc. 137 (2015) 13844–13850.
[59] Y. Mun, K. Kim, S. Kim, S. Lee, S. Lee, S. Kim, W. Choi, S.-K. Kim, J.W. Han, J. Lee, Appl. Catal., B 236 (2018) 154–161.
[60] X. Wei, Z. Yin, K. Lyu, Z. Li, J. Gong, G. Wang, L. Xiao, J. Lu, L. Zhuang, ACS Catal. 10 (2020) 4103–4111.
[61] A. Ozden, F. Li, F.P. García de Arquer, A. Rosas-Hernández, A. Thevenon, Y. Wang, S.-F. Hung, X. Wang, B. Chen, J. Li, ACS Energy Lett. 5 (2020) 2811–2818.
[62] Z. Han, R. Kortlever, H.-Y. Chen, J.C. Peters, T. Agapie, ACS Cent. Sci. 3 (2017) 853–859.
[63] M. Jun, D. Kim, M. Kim, M. Kim, T. Kwon, K. Lee, ACS Omega 7 (2022) 42655–42663.
[64] T.L. Soucy, W.S. Dean, J. Zhou, K.E. Rivera Cruz, C.C.L. McCrory, Acc. Chem. Res. 55 (2022) 252–261.
[65] P. Chen, Y. Wu, T.E. Rufford, L. Wang, G. Wang, Z. Wang, Mater. Today Chem. 27 (2023) 101328.
[66] D. Wakerley, S. Lamaison, F. Ozanam, N. Menguy, D. Mercier, P. Marcus, M. Fontecave, V. Mougel, Nat. Mater. 18 (2019) 1222–1227.
[67] Z. Xing, L. Hu, D.S. Ripatti, X. Hu, X. Feng, Nat. Commun. 12 (2021) 136.
[68] H.-Q. Liang, S. Zhao, X.-M. Hu, M. Ceccato, T. Skrydstrup, K. Daasbjerg, ACS Catal. 11 (2021) 958–966.
[69] F. Pan, Y. Yang, Energy Environ. Sci. 13 (2020) 2275–2309.
[70] T.K. Sau, A.L. Rogach, Adv. Mater. 22 (2010) 1781–1804.
[71] H. Xie, T. Wang, J. Liang, Q. Li, S. Sun, Nano Today 21 (2018) 41–54.
[72] I.J. Beyerlein, M.J. Demkowicz, A. Misra, B.P. Uberuaga, Prog. Mater. Sci. 74 (2015) 125–210.
[73] S. Verma, A.K. Mishra, J. Kumar, Acc. Chem. Res. 43 (2010) 79–91.
[74] K. Zhou, Y. Li, Angew. Chem., Int. Ed. 51 (2012) 602–613.
[75] Y. Wang, Z. Wang, C.-T. Dinh, J. Li, A. Ozden, M. Golam Kibria, A. Seifitokaldani, C.-S. Tan, C.M. Gabardo, M. Luo, H. Zhou, F. Li, Y. Lum, C. McCallum, Y. Xu, M. Liu, A. Proppe, A. Johnston, P. Todorovic, T.-T. Zhuang, D. Sinton, S.O. Kelley, E. H. Sargent, Nat. Catal. 3 (2020) 98–106.
[76] B. Zhang, J. Zhang, M. Hua, Q. Wan, Z. Su, X. Tan, L. Liu, F. Zhang, G. Chen, D. Tan, X. Cheng, B. Han, L. Zheng, G. Mo, J. Am. Chem. Soc. 142 (2020) 13606–13613.
[77] G.L. De Gregorio, T. Burdyny, A. Loiudice, P. Iyengar, W.A. Smith, R. Buonsanti, ACS Catal. 10 (2020) 4854–4862.
[78] H. Li, P. Yu, R. Lei, F. Yang, P. Wen, X. Ma, G. Zeng, J. Guo, F.M. Toma, Y. Qiu, S. M. Geyer, X. Wang, T. Cheng, W.S. Drisdell, Angew. Chem., Int. Ed. 60 (2021) 24838–24843.
[79] T. Sun, G. Zhang, D. Xu, X. Lian, H. Li, W. Chen, C. Su, Mater. Today Energy 12 (2019) 215–238.
[80] J. Zhang, Z. Li, S. Xia, T. Zhang, Y. Wang, Y. Wu, J. Wu, Chem. Commun. 57 (2021) 8276–8279.
[81] J. Zhang, Z. Liu, H. Guo, H. Lin, H. Wang, X. Liang, H. Hu, Q. Xia, X. Zou, X. Huang, ACS Appl. Mater. Interfaces 14 (2022) 19388–19396.
[82] K. Xiang, F. Zhu, Y. Liu, Y. Pan, X. Wang, X. Yan, H. Liu, Electrochem. Commun. 102 (2019) 72–77.
[83] H. Chen, A.D. Handoko, T. Wang, J. Qu, J. Xiao, X. Liu, D. Legut, Z. Wei Seh, Q. Zhang, ChemSusChem 13 (2020) 5690–5698.
[84] J. Jiang, B. Huang, R. Daiyan, B. Subhash, C. Tsounis, Z. Ma, C. Han, Y. Zhao, L.H. Effendi, L.C. Gallington, J.N. Hart, J.A. Scott, N.M. Bedford, Nano Energy 101 (2022) 107593.
[85] Y. Shang, L. Guo, Adv. Sci. 2 (2015) 1500140.
[86] R. Qin, N. Zheng, Chem 5 (2019) 1935–1937.
[87] M. Philip, A.R. Woldu, M.B. Akbar, H. Louis, H. Cong, Nanoscale 13 (2021) 3042–3048.
[88] Y. Bing, H. Liu, L. Zhang, D. Ghosh, J. Zhang, Chem. Soc. Rev. 39 (2010) 2184–2202.
[89] Z. Fang, Y. Wang, C. Liu, S. Chen, W. Sang, C. Wang, J. Zeng, Small 11 (2015) 2593–2605.
[90] Y. Wang, T. Gong, M. Lee, A.S. Hall, Curr. Opin. Electrochem. 30 (2021) 100796.
[91] S. Zhen, G. Zhang, D. Cheng, H. Gao, L. Li, X. Lin, Z. Ding, Z.-J. Zhao, J. Gong, Angew. Chem., Int. Ed. 61 (2022) e202201913.
[92] H.A. Gasteiger, S.S. Kocha, B. Sompalli, F.T. Wagner, Appl. Catal., B 56 (2005) 9–35.
[93] R. Schöllhorn, Angew. Chem., Int. Ed. 19 (1980) 983–1003.
[94] C. Kim, F. Dionigi, V. Beermann, X. Wang, T. Möller, P. Strasser, Adv. Mater. 31 (2019) 1805617.
[95] J. Greeley, I. Stephens, A. Bondarenko, T.P. Johansson, H.A. Hansen, T. Jaramillo, J. Rossmeisl, I. Chorkendorff, J.K. Nørskov, Nat. Chem. 1 (2009) 552–556.
[96] Y. Feng, W. An, Z. Wang, Y. Wang, Y. Men, Y. Du, ACS Sustainable Chem. Eng. 8 (2020) 210–222.
[97] Y. Du, W. An, J. Phys. Chem. C. 125 (2021) 9138–9149.
[98] S. Ma, M. Sadakiyo, M. Heima, R. Luo, R.T. Haasch, J.I. Gold, M. Yamauchi, P.J.A. Kenis, J. Am. Chem. Soc. 139 (2017) 47–50.
[99] S. Jia, Q. Zhu, H. Wu, M.E. Chu, S. Han, R. Feng, J. Tu, J. Zhai, B. Han, Chinese J. Catal. 41 (2020) 1091–1098.
[100] J. Shan, Y. Shi, H. Li, Z. Chen, C. Sun, Y. Shuai, Z. Wang, Chem. Eng. J. 433 (2022) 133769.
[101] T.T.H. Hoang, S. Verma, S. Ma, T.T. Fister, J. Timoshenko, A.I. Frenkel, P.J.A. Kenis, A.A. Gewirth, J. Am. Chem. Soc. 140 (2018) 5791–5797.
[102] L. Xiong, X. Zhang, H. Yuan, J. Wang, X. Yuan, Y. Lian, H. Jin, H. Sun, Z. Deng, D. Wang, J. Hu, H. Hu, J. Choi, J. Li, Y. Chen, J. Zhong, J. Guo, M.H. Rümmerli, L. Xu, Y. Peng, Angew. Chem., Int. Ed. 60 (2021) 2508–2518.
[103] Y. Ma, J. Yu, M. Sun, B. Chen, X. Zhou, C. Ye, Z. Guan, W. Guo, G. Wang, S. Lu, D. Xia, Y. Wang, Z. He, L. Zheng, Q. Yun, L. Wang, J. Zhou, P. Lu, J. Yin, Y. Zhao, Z. Luo, L. Zhai, L. Liao, Z. Zhu, R. Ye, Y. Chen, Y. Lu, S. Xi, B. Huang, C.-S. Lee, Z. Fan, Adv. Mater. 34 (2022) 2110607.
[104] A. Walsh, A.A. Sokol, J. Buckeridge, D.O. Scanlon, C.R.A. Catlow, Nat. Mater. 17 (2018) 958–964.
[105] H. Xiao, W.A. Goddard, T. Cheng, Y. Liu, Proc. Natl. Acad. Sci. U.S.A. 114 (2017) 6685–6688.
[106] C. Guo, Y. Guo, Y. Shi, X. Lan, Y. Wang, Y. Yu, B. Zhang, Angew. Chem., Int. Ed. 61 (2022) e202205909.
[107] C.-J. Chang, Y.-A. Lai, Y.-C. Chu, C.-K. Peng, H.-Y. Tan, C.-W. Pao, Y.-G. Lin, S.-F. Hung, H.-C. Chen, H.M. Chen, J. Am. Chem. Soc. 145 (2023) 6953–6965.
[108] J. Wang, Y. Chen, S. Zhang, C. Yang, J.-Y. Zhang, Y. Su, G. Zheng, X. Fang, Small 18 (2022) 2202238.
[109] F. Yang, W. Fang, Q. Wang, P. Deng, B.Y. Xia, ACS Sustainable Chem. Eng. 10 (2022) 4677–4682.
[110] H. Mistry, A.S. Varela, C.S. Bonifacio, I. Zegkinoglou, I. Sinev, Y.-W. Choi, K. Kisslinger, E.A. Stach, J.C. Yang, P. Strasser, B.R. Cuenya, Nat. Commun. 7 (2016) 12123.
[111] T.-C. Chou, C.-C. Chang, H.-L. Yu, W.-Y. Yu, C.-L. Dong, J.-J. Velasco-Vélez, C.-H. Chuang, L.-C. Chen, J.-F. Lee, J.-M. Chen, H.-L. Wu, J. Am. Chem. Soc. 142 (2020) 2857–2867.
[112] A. Hauch, R. Küngas, P. Blennow, A.B. Hansen, J.B. Hansen, B.V. Mathiesen, M. B. Mogensen, Science 370 (2020) eaba6118.
[113] R. Sander, Atmos. Chem. Phys. Discuss 14 (2014) 29615–30521.
[114] A. Tamimi, E.B. Rinker, O.C. Sandall, J. Chem. Eng. Data 39 (1994) 330–332.
[115] S.S. Bhargava, F. Proietto, D. Azmoodeh, E.R. Cofell, D.A. Henckel, S. Verma, C.J. Brooks, A.A. Gewirth, P.J. Kenis, ChemElectroChem 7 (2020) 2001–2011.
[116] K.K. Patra, C.S. Gopinath, Chem. Commun. 59 (2023) 6774–6795.
[117] F.P. García de Arquer, C.-T. Dinh, A. Ozden, J. Wicks, C. McCallum, A.R. Kirmani, D.-H. Nam, C. Gabardo, A. Seifitokaldani, X. Wang, Y.C. Li, F. Li, J. Edwards, L.J. Richter, S.J. Thorpe, D. Sinton, E.H. Sargent, Science 367 (2020) 661–666.
[118] C.-T. Dinh, T. Burdyny, M.G. Kibria, A. Seifitokaldani, C.M. Gabardo, F.P.G.D. Arquer, A. Kiani, J.P. Edwards, P.D. Luna, O.S. Bushuyev, C. Zou, R. Quintero-Bermudez, Y. Pang, D. Sinton, E.H. Sargent, Science 360 (2018) 783–787.
[119] J. Lin, Y. Zhang, P. Xu, L. Chen, Mater. Rep.: Energy 3 (2023) 100194.
[120] D.M. Weekes, D.A. Salvatore, A. Reyes, A. Huang, C.P. Berlinguette, Acc. Chem. Res. 51 (2018) 910–918.
[121] M. de Jesus Gálvez-Vázquez, P. Moreno-García, H. Xu, Y. Hou, H. Hu, I.Z. Montiel, A.V. Rudnev, S. Alinejad, V. Grozovski, B.J. Wiley, M. Arenz, P. Broekmann, ACS Catal. 10 (2020) 13096–13108.
[122] Y.C. Tan, W.K. Quek, B. Kim, S. Sugiarto, J. Oh, D. Kai, ACS Energy Lett. 7 (2022) 2012–2023.
[123] F. Bienen, D. Kopljar, A. Löwe, S. Geiger, N. Wagner, E. Klemm, K.A. Friedrich, ACS Sustainable Chem. Eng. 8 (2020) 13759–13768.
[124] E.W. Lees, B.A.W. Mowbray, F.G.L. Parlane, C.P. Berlinguette, Nat. Rev. Mater. 7 (2022) 55–64.

[125] E.J. Dufek, T.E. Lister, M.E. McIlwain, J. Appl. Electrochem. 41 (2011) 623–631.
[126] S. Liang, N. Altaf, L. Huang, Y. Gao, Q. Wang, J. CO_2 Util. 35 (2020) 90—105.
[127] K. Liu, W.A. Smith, T. Burdyny, ACS Energy Lett. 4 (2019) 639–643.
[128] D. Higgins, C. Hahn, C. Xiang, T.F. Jaramillo, A.Z. Weber, ACS Energy Lett. 4 (2018) 317–324.
[129] J. Yu, J. Xiao, Y. Ma, J. Zhou, P. Lu, K. Wang, Y. Yan, J. Zeng, Y. Wang, S. Song, Z. Fan, Chem Catal. 3 (2023) 100670.
[130] T. Zhang, J. Zhou, T. Luo, J.-Q. Lu, Z. Li, X. Weng, F. Yang, Chem. Eur. J. 29 (2023) e202301455.
[131] M. Sassenburg, M. Kelly, S. Subramanian, W.A. Smith, T. Burdyny, ACS Energy Lett. 8 (2023) 321–331.
[132] M. Jouny, W. Luc, F. Jiao, Ind. Eng. Chem. Res. 57 (2018) 2165–2177.
[133] S. Verma, B. Kim, H.-R.-M. Jhong, S. Ma, P.J.A. Kenis, ChemSusChem 9 (2016) 1972–1979.
[134] B. Endrodi, E. Kecsenovity, A. Samu, F. Darvas, R. Jones, V. Török, A. Danyi, C. Janáky, ACS Energy Lett. 4 (2019) 1770–1777.
[135] J. Zhang, W. Luo, A. Züttel, J. Catal. 385 (2020) 140–145.
[136] W.H. Lee, K. Kim, C. Lim, Y.-J. Ko, Y.J. Hwang, B.K. Min, U. Lee, H.-S. Oh, J. Mater. Chem. A 9 (2021) 16169–16177.
[137] K.P. Kuhl, E.R. Cave, D.N. Abram, T.F. Jaramillo, Energy Environ. Sci. 5 (2012) 7050–7059.
[138] A. Loiudice, P. Lobaccaro, E.A. Kamali, T. Thao, B.H. Huang, J.W. Ager, R. Buonsanti, Angew. Chem., Int. Ed. 55 (2016) 5789–5792.
[139] S. Sen, D. Liu, G.T.R. Palmore, ACS Catal. 4 (2014) 3091–3095.
[140] I. Takahashi, O. Koga, N. Hoshi, Y. Hori, J. Electroanal. Chem. 533 (2002) 135–143.
[141] H. Yano, T. Tanaka, M. Nakayama, K. Ogura, J. Electroanal. Chem. 565 (2004) 287–293.
[142] A. Ozden, Y. Wang, F. Li, M. Luo, J. Sisler, A. Thevenon, A. Rosas-Hernández, T. Burdyny, Y. Lum, H. Yadegari, T. Agapie, J.C. Peters, E.H. Sargent, D. Sinton, Joule 5 (2021) 706–719.
[143] X. Chen, J. Chen, N.M. Alghoraibi, D.A. Henckel, R. Zhang, U.O. Nwabara, K.E. Madsen, P.J.A. Kenis, S.C. Zimmerman, A.A. Gewirth, Nat. Catal. 4 (2021) 20–27.
[144] W. Li, Z. Yin, Z. Gao, G. Wang, Z. Li, F. Wei, X. Wei, H. Peng, X. Hu, L. Xiao, J. Lu, L. Zhuang, Nat. Energy 7 (2022) 835–843.
[145] D.-H. Nam, O. Shekhah, A. Ozden, C. McCallum, F. Li, X. Wang, Y. Lum, T. Lee, J. Li, J. Wicks, A. Johnston, D. Sinton, M. Eddaoudi, E.H. Sargent, Adv. Mater. 34 (2022) 2207088.
[146] C.-T. Dinh, T. Burdyny, M.G. Kibria, A. Seifitokaldani, C.M. Gabardo, F.P. García de Arquer, A. Kiani, J.P. Edwards, P. De Luna, O.S. Bushuyev, C. Zou, R. Quintero-Bermudez, Y. Pang, D. Sinton, E.H. Sargent, Science 360 (2018) 783–787.
[147] M. Jouny, W. Luc, F. Jiao, Nat. Catal. 1 (2018) 748–755.
[148] C.-T. Dinh, Y.C. Li, E.H. Sargent, Joule 3 (2019) 13–15.
[149] C.P. O'Brien, R.K. Miao, S. Liu, Y. Xu, G. Lee, A. Robb, J.E. Huang, K. Xie, K. Bertens, C.M. Gabardo, J.P. Edwards, C.-T. Dinh, E.H. Sargent, D. Sinton, ACS Energy Lett. 6 (2021) 2952–2959.
[150] B. Pan, J. Fan, J. Zhang, Y. Luo, C. Shen, C. Wang, Y. Wang, Y. Li, ACS Energy Lett. 7 (2022) 4224–4231.
[151] K. Xie, R.K. Miao, A. Ozden, S. Liu, Z. Chen, C.-T. Dinh, J.E. Huang, Q. Xu, C.M. Gabardo, G. Lee, J.P. Edwards, C.P. O'Brien, S.W. Boettcher, D. Sinton, E.H. Sargent, Nat. Commun. 13 (2022) 3609.
[152] Y. Xie, P. Ou, X. Wang, Z. Xu, Y.C. Li, Z. Wang, J.E. Huang, J. Wicks, C. McCallum, N. Wang, Y. Wang, T. Chen, B.T.W. Lo, D. Sinton, J.C. Yu, Y. Wang, E.H. Sargent, Nat. Catal. 5 (2022) 564–570.
[153] D.S. Ripatti, T.R. Veltman, M.W. Kanan, Joule 3 (2019) 240–256.
[154] D. Wakerley, S. Lamaison, J. Wicks, A. Clemens, J. Feaster, D. Corral, S.A. Jaffer, A. Sarkar, M. Fontecave, E.B. Duoss, S. Baker, E.H. Sargent, T.F. Jaramillo, C. Hahn, Nat. Energy 7 (2022) 130–143.
[155] E. Jeng, F. Jiao, React. Chem. Eng. 5 (2020) 1768–1775.
[156] M.R. Singh, E.L. Clark, A.T. Bell, Phys. Chem. Chem. Phys. 17 (2015) 18924–18936.
[157] H. Rabiee, L. Ge, X. Zhang, S. Hu, M. Li, Z. Yuan, Energy Environ. Sci. 14 (2021) 1959–2008.
[158] N. Gupta, M. Gattrell, B. MacDougall, J. Appl. Electrochem. 36 (2006) 161–172.
[159] S. Verma, Y. Hamasaki, C. Kim, W. Huang, S. Lu, H.-R.-M. Jhong, A.A. Gewirth, T. Fujigaya, N. Nakashima, P.J. Kenis, ACS Energy Lett. 3 (2017) 193–198.
[160] M.E. Leonard, L.E. Clarke, A. Forner-Cuenca, S.M. Brown, F.R. Brushett, ChemSusChem 13 (2020) 400–411.
[161] D.G. Wheeler, B.A. Mowbray, A. Reyes, F. Habibzadeh, J. He, C.P. Berlinguette, Energy Environmental Science 13 (2020) 5126–5134.
[162] J.A. Rabinowitz, M.W. Kanan, Nat. Commun. 11 (2020) 1–3.
[163] M. Ma, E.L. Clark, K.T. Therkildsen, S. Dalsgaard, I. Chorkendorff, B. Seger, Energy Environ. Sci. 13 (2020) 977–985.
[164] Y.C. Tan, K.B. Lee, H. Song, J. Oh, Joule 4 (2020) 1104–1120.
[165] A. Reyes, R.P. Jansonius, B.A. Mowbray, Y. Cao, D.G. Wheeler, J. Chau, D.J. Dvorak, C.P. Berlinguette, ACS Energy Lett. 5 (2020) 1612–1618.
[166] Z. Yin, H. Peng, X. Wei, H. Zhou, J. Gong, M. Huai, L. Xiao, G. Wang, J. Lu, L. Zhuang, Energy Environ. Sci. 12 (2019) 2455–2462.
[167] L. Xue, Z. Gao, T. Ning, W. Li, J. Li, J. Yin, L. Xiao, G. Wang, L. Zhuang, Angew. Chem., Int. Ed. 135 (2023) e202309519.
[168] C. Chen, Y. Li, P. Yang, Joule 5 (2021) 737–742.
[169] M. Kolen, D. Ripepi, W.A. Smith, T. Burdyny, F.M. Mulder, ACS Catal. 12 (2022) 5726–5735.
[170] Z. Xing, K. Shi, X. Hu, X. Feng, J. Energy Chem. 66 (2022) 45–51.
[171] W.H. Lee, C. Lim, S.Y. Lee, K.H. Chae, C.H. Choi, U. Lee, B.K. Min, Y.J. Hwang, H.-S. Oh, Nano Energy 84 (2021) 105859.
[172] Y. Zhao, X. Zu, R. Chen, X. Li, Y. Jiang, Z. Wang, S. Wang, Y. Wu, Y. Sun, Y. Xie, J. Am. Chem. Soc. 144 (2022) 10446–10454.
[173] X. Zhang, Z. Zhou, J. Phys. Chem. C. 126 (2022) 3820–3829.
[174] J. Wei, Y. Yang, J. Liu, B. Xiong, J. CO_2 Util. 64 (2022) 102165.
[175] L. Chen, X. Zhang, A. Chen, S. Yao, X. Hu, Z. Zhou, Chinese J. Catal. 43 (2022) 11–32.
[176] O.A. Moses, W. Chen, M.L. Adam, Z. Wang, K. Liu, J. Shao, Z. Li, W. Li, C. Wang, H. Zhao, C.H. Pang, Z. Yin, X. Yu, Mater. Rep.: Energy 1 (2021) 100049.
[177] J. Wei, X. Chu, X.-Y. Sun, K. Xu, H.-X. Deng, J. Chen, Z. Wei, M. Lei, InfoMat 1 (2019) 338–358.
[178] M.I. Jordan, T.M. Mitchell, Science 349 (2015) 255–260.
[179] H. Zhu, S. Liu, J. Yu, Q. Chen, X. Mao, T. Wu, Nanoscale 15 (2023) 8416–8423.
[180] J.R. Kitchin, Nat. Catal. 1 (2018) 230–232.
[181] W. Liao, P. Liu, Catal. Sci. Technol. 12 (2022) 3836–3845.
[182] M. Zhong, K. Tran, Y. Min, C. Wang, Z. Wang, C.-T. Dinh, P. De Luna, Z. Yu, A.S. Rasouli, P. Brodersen, S. Sun, O. Voznyy, C.-S. Tan, M. Askerka, F. Che, M. Liu, A. Seifitokaldani, Y. Pang, S.-C. Lo, A. Ip, Z. Ulissi, E.H. Sargent, Nature 581 (2020) 178–183.
[183] Z. Sun, H. Yin, K. Liu, S. Cheng, G.K. Li, S. Kawi, H. Zhao, G. Jia, Z. Yin, SmartMat 3 (2022) 68–83.
[184] D. Wu, J. Zhang, M.-J. Cheng, Q. Lu, H. Zhang, J. Phys. Chem. C. 125 (2021) 15363–15372.
[185] Z. Yang, W. Gao, Q. Jiang, J. Mater. Chem. A 8 (2020) 17507–17515.
[186] H. Feng, H. Ding, P. He, S. Wang, Z. Li, Z. Zheng, Y. Yang, M. Wei, X. Zhang, J. Mater. Chem. A 10 (2022) 18803–18811.
[187] K. Tran, Z.W. Ulissi, Nat. Catal. 1 (2018) 696–703.
[188] E. Hu, C. Liu, W. Zhang, Q. Yan, J. Phys. Chem. C. 127 (2023) 882–893.
[189] L. Wu, T. Guo, T. Li, J. Mater. Chem. A 8 (2020) 19290–19299.
[190] M. Tamtaji, H. Gao, M.D. Hossain, P.R. Galligan, H. Wong, Z. Liu, H. Liu, Y. Cai, W.A. Goddard, Z. Luo, J. Mater. Chem. A 10 (2022) 15309–15331.
[191] D. Roy, S.C. Mandal, B. Pathak, J. Phys. Chem. Lett 13 (2022) 5991–6002.
[192] Q. Zhu, Y. Gu, X. Liang, X. Wang, J. Ma, ACS Catal. 12 (2022) 12336–12348.
[193] X. Wan, Z. Zhang, H. Niu, Y. Yin, C. Kuai, J. Wang, C. Shao, Y. Guo, J. Phys. Chem. Lett 12 (2021) 6111–6118.
[194] Y. Guo, X. He, Y. Su, Y. Dai, M. Xie, S. Yang, J. Chen, K. Wang, D. Zhou, C. Wang, J. Am. Chem. Soc. 143 (2021) 5755–5762.
[195] M. Ramdin, B. De Mot, A.R.T. Morrison, T. Breugelmans, L.J.P. van den Broeke, J.P.M. Trusler, R. Kortlever, W. de Jong, O.A. Moultos, P. Xiao, P.A. Webley, T.J. H. Vlugt, Ind. Eng. Chem. Res. 60 (2021) 17862–17880.
[196] X. Wang, J.F. de Araújo, W. Ju, A. Bagger, H. Schmies, S. Kühl, J. Rossmeisl, P. Strasser, Nat. Nanotechnol. 14 (2019) 1063–1070.
[197] R. Chen, H.-Y. Su, D. Liu, R. Huang, X. Meng, X. Cui, Z.-Q. Tian, D.H. Zhang, D. Deng, Angew. Chem., Int. Ed. 59 (2020) 154–160.
[198] M. He, C. Li, H. Zhang, X. Chang, J.G. Chen, W.A. Goddard, M.-J. Cheng, B. Xu, Q. Lu, Nat. Commun. 11 (2020) 3844.
[199] H. Yadegari, A. Ozden, T. Alkayyali, V. Soni, A. Thevenon, A. Rosas-Hernández, T. Agapie, J.C. Peters, E.H. Sargent, D. Sinton, ACS Energy Lett. 6 (2021) 3538–3544.
[200] G. Papanikolaou, G. Centi, S. Perathoner, P. Lanzafame, ACS Catal. 12 (2022) 2861–2876.
[201] A.N. Biswas, Z. Xie, R. Xia, S. Overa, F. Jiao, J.G. Chen, ACS Energy Lett. 7 (2022) 2904–2910.
[202] Y. Liu, Y. Li, Y. Chen, T. Qu, C. Shu, X. Yang, H. Zhu, S. Guo, S. Zhao, T. Asefa, Y. Liu, J. Mater. Chem. A 8 (2020) 8329–8336.
[203] Y. Cheng, P. Hou, X. Wang, P. Kang, Acc. Chem. Res. 55 (2022) 231–240.
[204] S. Zhang, C. Chen, K. Li, H. Yu, F. Li, J. Mater. Chem. A 9 (2021) 18785–18792.
[205] H. Guzmán, N. Russo, S. Hernández, Green Chem. 23 (2021) 1896–1920.
[206] M.S. Sajna, S. Zavahir, A. Popelka, P. Kasak, A. Al-Sharshani, U. Onwusogh, M. Wang, H. Park, D.S. Han, J. Environ. Chem. Eng. 11 (2023) 110467.
[207] Y. Gao, L. Neal, D. Ding, W. Wu, C. Baroi, A.M. Gaffney, F. Li, ACS Catal. 9 (2019) 8592–8621.
[208] M. Ma, S. Kim, I. Chorkendorff, B. Seger, Chem. Sci. 11 (2020) 8854–8861.
[209] O. Alvizo, L.J. Nguyen, C.K. Savile, J.A. Bresson, S.L. Lakhapatri, E.O.P. Solis, R.J. Fox, J.M. Broering, M.R. Benoit, S.A. Zimmerman, S.J. Novick, J. Liang, J.J. Lalonde, Proc. Natl. Acad. Sci. U.S.A. 111 (2014) 16436–16441.
[210] P. Zhu, H. Wang, Nat. Catal. 4 (2021) 943–951.
[211] Y. Xu, J.P. Edwards, J. Zhong, C.P. O'Brien, C.M. Gabardo, C. McCallum, J. Li, C.-T. Dinh, E.H. Sargent, D. Sinton, Energy Environ. Sci. 13 (2020) 554–561.
[212] A. Prajapati, R. Sartape, M.T. Galante, J. Xie, S.L. Leung, I. Bessa, M.H.S. Andrade, R.T. Somich, M.V. Rebouças, G.T. Hutras, N. Diniz, M.R. Singh, Energy Environ. Sci. 15 (2022) 5105–5117.
[213] M.G. Kibria, J.P. Edwards, C.M. Gabardo, C.-T. Dinh, A. Seifitokaldani, D. Sinton, E.H. Sargent, Adv. Mater. 31 (2019) 1807166.
[214] W. Lai, Y. Qiao, J. Zhang, Z. Lin, H. Huang, Energy Environ. Sci. 15 (2022) 3603–3629.
[215] H. Yang, J.J. Kaczur, S.D. Sajjad, R.I. Masel, J. CO_2 Util. 20 (2017) 208–217.
[216] D. Steward, T. Ramsden, J. Zuboy, H2A Production Model, Version 2 User Guide, National Renewable Energy Lab.(NREL), Golden, CO (United States), 2008.

[217] A. Wiheeb, Z. Helwani, J. Kim, M. Othman, Sep. Purif. Rev. 45 (2016) 108–121.
[218] S. Jin, Z. Hao, K. Zhang, Z. Yan, J. Chen, Angew. Chem., Int. Ed. 60 (2021) 20627—20648.
[219] Z. Chen, X. Zhang, W. Liu, M. Jiao, K. Mou, X. Zhang, L. Liu, Energy Environ. Sci. 14 (2021) 2349–2356.
[220] T. Möller, W. Ju, A. Bagger, X. Wang, F. Luo, T. Ngo Thanh, A.S. Varela, J. Rossmeisl, P. Strasser, Energy Environ. Sci. 12 (2019) 640–647.
[221] Y. Kuang, H. Rabiee, L. Ge, T.E. Rufford, Z. Yuan, J. Bell, H. Wang, Energy Environ. Sci. (2023) e12596.
[222] C. Chen, Y. Li, S. Yu, S. Louisia, J. Jin, M. Li, M.B. Ross, P. Yang, Joule 4 (2020) 1688–1699.
[223] N.S. Romero Cuellar, C. Scherer, B. Kaçkar, W. Eisenreich, C. Huber, K. Wiesner-Fleischer, M. Fleischer, O. Hinrichsen, J. CO_2 Util. 36 (2020) 263–275.
[224] N.M. Haegel, R. Margolis, T. Buonassisi, D. Feldman, A. Froitzheim, R. Garabedian, M. Green, S. Glunz, H.-M. Henning, B. Holder, I. Kaizuka, B. Kroposki, K. Matsubara, S. Niki, K. Sakurai, R.A. Schindler, W. Tumas, E.R. Weber, G. Wilson, M. Woodhouse, S. Kurtz, Science 356 (2017) 141–143.
[225] H.W. Ryan, B. Mark, 2015 Wind Technologies Market Report, 2016.
[226] A. Raksajati, M.T. Ho, D.E. Wiley, Ind. Eng. Chem. Res. 52 (2013) 16887–16901.
[227] J.M. Spurgeon, B. Kumar, Energy Environ. Sci. 11 (2018) 1536–1551.
[228] Y. Pang, J. Li, Z. Wang, C.-S. Tan, P.-L. Hsieh, T.-T. Zhuang, Z.-Q. Liang, C. Zou, X. Wang, P. De Luna, Nat. Catal. 2 (2019) 251–258.
[229] N. Theaker, J.M. Strain, B. Kumar, J.P. Brian, S. Kumari, J.M. Spurgeon, Electrochim. Acta 274 (2018) 1–8.